



**HAL**  
open science

## pH-Controlled Self-Assembled Fibrillar Network Hydrogels: Evidence of Kinetic Control of the Mechanical Properties

Ghazi Ben Messaoud, Patrick Le Griel, Daniel Hermida-Merino, Sophie L. K. W. Roelants, Wim Soetaert, Christian Victor Stevens, Niki Baccile

► **To cite this version:**

Ghazi Ben Messaoud, Patrick Le Griel, Daniel Hermida-Merino, Sophie L. K. W. Roelants, Wim Soetaert, et al.. pH-Controlled Self-Assembled Fibrillar Network Hydrogels: Evidence of Kinetic Control of the Mechanical Properties. *Chemistry of Materials*, 2019, 31 (13), pp.4817-4830. 10.1021/acs.chemmater.9b01230 . hal-02160875

**HAL Id: hal-02160875**

**<https://hal.sorbonne-universite.fr/hal-02160875>**

Submitted on 20 Jun 2019

**HAL** is a multi-disciplinary open access archive for the deposit and dissemination of scientific research documents, whether they are published or not. The documents may come from teaching and research institutions in France or abroad, or from public or private research centers.

L'archive ouverte pluridisciplinaire **HAL**, est destinée au dépôt et à la diffusion de documents scientifiques de niveau recherche, publiés ou non, émanant des établissements d'enseignement et de recherche français ou étrangers, des laboratoires publics ou privés.

1  
2  
3  
4  
5  
6  
7  
8  
9  
10  
11  
12  
13  
14  
15  
16  
17  
18  
19  
20  
21  
22  
23  
24

# **pH-controlled self-assembled fibrillar network (SAFiN) hydrogels: evidence of a kinetic control of the mechanical properties**

Ghazi Ben Messaoud,<sup>a,†</sup> Patrick Le Griel,<sup>a</sup> Daniel Hermida-Merino,<sup>b</sup> Sophie L. K. W. Roelants,<sup>c,d</sup> Wim Soetaert,<sup>c</sup> Christian Victor Stevens,<sup>e</sup> Niki Baccile<sup>a,\*</sup>

<sup>a</sup> Sorbonne Université, Centre National de la Recherche Scientifique, Laboratoire de Chimie de la Matière Condensée de Paris, LCMCP, F-75005 Paris, France

<sup>†</sup> Current address: DWI- Leibniz Institute for Interactive Materials, Forckenbeckstrasse 50, 52056 Aachen, Germany

<sup>b</sup> Netherlands Organisation for Scientific Research (NWO), DUBBLE@ESRF BP CS40220, 38043 Grenoble, France

<sup>c</sup> Ghent University, Centre for Industrial Biotechnology and Biocatalysis (InBio.be), Coupure Links 653, Ghent, Oost-Vlaanderen, BE 9000

<sup>d</sup> Bio Base Europe Pilot Plant, Rodenhuzekaai 1, Ghent, Oost-Vlaanderen, BE 9000

<sup>e</sup> SynBioC, Department of Green Chemistry and Technology, Ghent University, Coupure Links 653, 9000 Ghent, Belgium.

## **\* Corresponding author:**

Dr. Niki Baccile

E-mail address: niki.baccile@upmc.fr

Phone: 00 33 1 44 27 56 77

## 25 **Abstract**

26 Control of the nucleation and growth process in self-assembled fibrillary networks (SAFiN)  
27 with the goal of preparing physical hydrogels from low molecular weight gelators (LMWG) is  
28 well-established but mainly for temperature-driven hydrogelators. In the presence of other  
29 stimuli, like pH, the fundamental knowledge behind gel formation still lacks. In particular,  
30 whether pH affects nucleation and growth of the fibers and how this aspect could be related to  
31 the stability of the hydrogel is still matter of debate. In this work, we establish a precise  
32 relationship between the pH change rate during the micelle-to-fiber transition, observed for  
33 stearic acid sophorolipids - a bolaform microbial glycolipid – and supersaturation. We show  
34 that tough SAFiN hydrogels are obtained for slow pH change rates, when supersaturation is  
35 low, while weak gels, or even phase separation through powder precipitation, are obtained upon  
36 fast pH change. Interestingly, these results are independent of the pH change method, may it be  
37 through manual variation using HCl, or by using the internal hydrolysis of glucono- $\delta$ -lactone  
38 (GDL), the latter being currently acknowledged as a unique way to systematically obtain tough  
39 gel through internal pH change.

40

## 41 **Introduction**

42 The development of soft stimuli-responsive materials is a topic that has gained much  
43 attention in the past decades for the applications in many fields including tissue engineering,  
44 cosmetics, food and environmental science<sup>1-8</sup> and in relationship to the most recent materials'  
45 processing techniques, like 3D<sup>6</sup> and 4D printing.<sup>9</sup> In this field, low molecular weight gelators  
46 (LMWG),<sup>10,11</sup> small compounds commonly forming self-assembled fibrillary network (SAFiN)  
47 hydro- or organogels, attract a large interest for their potentially infinite possibilities in terms  
48 of the (molecular) function - (gel) property. The gelation is generally driven by weak  
49 interactions and can be triggered by numerous stimuli like temperature,<sup>12</sup> pH,<sup>13</sup> salt<sup>14</sup> or  
50 enzymes.<sup>15</sup> In this class of materials, fluorenyl-9-methoxycarbonyl (Fmoc) amino acid  
51 derivatives are one of the most popular class of LMWG but peptides, peptide amphiphiles and  
52 glycolipids<sup>16-20</sup> are also largely explored.

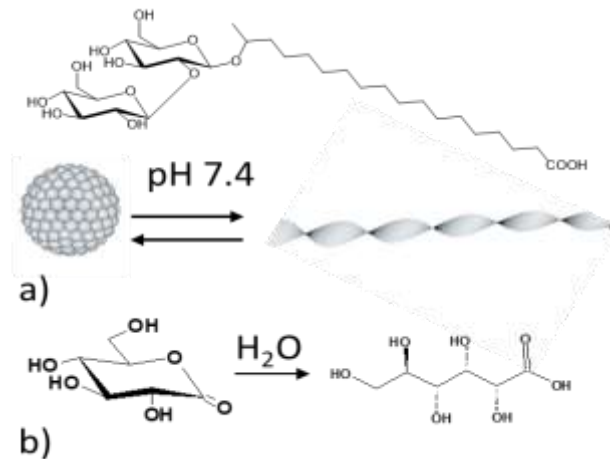
53 Temperature-driven SAFiN hydro- and organogels are by far the most common systems  
54 benefitting of the largest knowledge. Their mechanisms of formation and relationship between  
55 the gel mechanical properties and fiber nucleation/growth phenomena are well-understood.  
56 Supersaturation, driven by large temperature variations between the sol and gel phases, is  
57 responsible for high degrees of fiber branching, leading to gels with poor mechanical  
58 properties.<sup>21-24</sup> However, when it comes to the preparation of homogenous SAFiN hydrogels

59 triggered by pH as external stimulus, control of pH variation and of mechanical properties is  
60 still challenging. Several approaches, like generation of carboxylic acids during anhydrides  
61 hydrolysis<sup>25</sup> or UV irradiation of a photoacid generator<sup>26</sup> were developed as better alternatives  
62 to an obvious manual addition of the acid. However, since a decade, it is commonly  
63 acknowledged that use of glucono- $\delta$ -lactone (GDL, Figure 1b) is a straightforward, economic  
64 and smart approach: *in situ* release of gluconic acid during the hydrolysis of GDL promotes the  
65 formation of homogeneous SAFiN hydrogels.<sup>2,16,27,28</sup> However, whichever the method of  
66 acidification, the mechanisms of pH variation in relationship to the mechanical strength of the  
67 gel are not fully understood. This is particularly true for hydrogels prepared by manual pH  
68 change and of which the reported variations in terms of mechanical properties are also ascribed  
69 to the differences in shear induced by mixing during gel formation.<sup>29</sup> Even for GDL, such a  
70 relationship is not obvious and it is generally assumed that the final pH is practically the main  
71 parameter that controls the mechanical properties of the hydrogels.<sup>2,30,31</sup>

72 Recently, we have described the pH-induced fibrillation of the stearic derivative of  
73 acidic sophorolipids (SLC18:0, Figure 1a).<sup>32</sup> Sophorolipids are the most common, abundant  
74 and commercially-available microbial glycolipid biosurfactant in the literature,<sup>33,34</sup> with  
75 interesting self-assembly properties<sup>35-37</sup> and a wide range of applications for their low  
76 environmental impact, low cytotoxicity and good antimicrobial properties.<sup>33,34,38</sup> SLC18:0 is  
77 known to undergo a pH-driven micelle-to-fiber (twisted ribbon) phase transition at pH  $\sim$ 7.4  
78 (Figure 1a), below which this compound forms a SAFiN, although the formation of a hydrogel  
79 was never reported. To the best of our knowledge, in the broader field of glycolipid  
80 biosurfactants, only cellobioselipids and non-acidic symmetrical sophorolipids were shown to  
81 have gelling properties.<sup>39-41</sup>

82 If this compound could be expected to form a SAFiN hydrogel, which we show as the  
83 first result of this work, we also report an unprecedented role of the kinetics of pH variation to  
84 control the hydrogel homogeneity and to improve its mechanical properties. In contrast to the  
85 abundant literature on pH-driven LMWG hydrogels (often composed of Fmoc-derivatives), we  
86 show that both heterogeneous (through external HCl addition) and homogeneous (through  
87 internal GDL hydrolysis) acidification can induce the formation of homogeneous SAFiN  
88 hydrogels with comparable mechanical properties. We show that fine tuning of the acidification  
89 rate, using either HCl or GDL, controls the formation of a strong (homogeneous SAFiN), weak  
90 gel or even no gel at all, due to the formation of spherulites. By combining rheology, multi-  
91 scale (from nm to mm) structural analysis and exploring the pH-induced sol-gel transition by  
92 nuclear magnetic resonance (NMR) in solution, we propose that the formation of SLC18:0

93 hydrogels is not driven by the final pH but it is a diffusion-limited process. Under these  
94 circumstances, the method of acidification (external or internal) is not as important as initially  
95 imagined, because supersaturation plays a much more crucial role in the nucleation and growth  
96 mechanisms of the fibers during pH variation, in analogy to what is known in temperature-  
97 driven LMWG SAFiN.<sup>21,42-44</sup> Slow pH variation kinetics promote homogeneous fibrillation and  
98 tough hydrogels while fast kinetics induce spherulite formation and phase separation.  
99



100  
101 **Figure 1 – a) Chemical structure of SLC18:0 microbial glycolipid and its pH-driven assembly from micelles**  
102 **to fibers and b) hydrolysis of glucono- $\delta$ -lactone (GDL) to gluconic acid in water.**

103

104

## 105 **Experimental Section**

106 *Chemicals.* SLC18:0 ( $M_w = 624.8 \text{ g}\cdot\text{mol}^{-1}$ ) was obtained from SLC18:1 (Soliance, now  
107 Givaudan Active Beauty, France). The monounsaturated SLC18:1 was first hydrolyzed in an  
108 alkaline medium and the pH is then adjusted to  $\sim 4.5$  to obtain the deacetylated open acidic form  
109 and finally recovered using method 1 as reported previously.<sup>45</sup> The fully saturated SLC18:0  
110 was then obtained by a chemical modification step described elsewhere.<sup>32</sup> Glucono- $\delta$ -lactone  
111 (GDL,  $M_w = 178.1 \text{ g}\cdot\text{mol}^{-1}$ ) was purchased from Sigma Aldrich. 5 M NaOH and HCl stock  
112 solutions were respectively prepared by the dissolution of an appropriate amount of solid  
113 sodium hydroxide pellets (Sigma Aldrich) in water and by diluting 37 w% hydrochloric acid  
114 (Sigma Aldrich) in water. All solutions were prepared with Milli-Q-grade water.

115  
116 *Preparation of the hydrogels.* The general method to prepare the hydrogels consists in  
117 dispersing a given amount of SLC18:0 (in wt%) in water at the desired concentration, followed  
118 by sonication during 1-2 minutes, to break up the aggregated powder. The pH of the solution is  
119 increased to pH  $\sim 11$  under gentle magnetic stirring with few  $\mu\text{L}$  of 5 M NaOH (generally  
120 between 5  $\mu\text{L}$  and 20  $\mu\text{L}$ , according to the sample concentration, for a typical volume of 1 mL).  
121 The solution, turbid at the equilibrium pH, becomes mostly clear at basic pH, as discussed in  
122 previous work,<sup>32</sup> although slight turbidity can occur above pH 11 due to the formation of  
123 platelets.<sup>46</sup> Hydrogels are then obtained by acidification of the basic solution. However, the  
124 method to decrease the pH is critical for the hydrogel stability and properties. We present three  
125 methods of acidification, of which two of them are classical in the literature, while the third  
126 was specifically developed in this work.

127 *1) Manual acidification using HCl.* Manual acidification is a simple and classical  
128 approach to decrease the pH. Despite its optimization to this specific system, one should be  
129 careful to use it to obtain SLC18:0 hydrogels, because it lacks of precision and reproducibility.  
130 Briefly, solutions of 1 M and 0.5 M of HCl are used to manually acidify the SLC18:0 solution  
131 (values here are intended for a typical 1 mL solution). pH can be varied rapidly using 1 M HCl  
132 solution until pH  $\sim 7.4$ . Then 2  $\mu\text{L}$  of a 0.5 M HCl (for  $SL \leq 2.5 \text{ wt}\%$ ) or a 1 M HCl solution  
133 (for  $SL > 2.5 \text{ wt}\%$ ) are added dropwise under gentle stirring ( $\sim 100 \text{ rpm}$ ) using a magnetic bar.  
134 If small aggregates appear in solution, the sample must be sonicated between each added aliquot  
135 until the aggregates dissolve. The solution becomes then more and more turbid, but  
136 homogeneous. The stirring rate of the sample should be increased ( $> 300 \text{ rpm}$ ) due to the rise  
137 of the solution viscosity. Under these conditions, one can keep adding HCl until the desired  
138 final pH is reached (tough gels are generally obtained at pH  $\sim 6$ ). If these steps are not performed

139 correctly, one obtains a biphasic system composed of a precipitate and a slightly turbid aqueous  
140 phase at already pH ~ 7 and pH should be increased again to solubilize the sample and start the  
141 acidification step again. Regeneration of the sample generates larger amounts of salt (here,  
142 NaCl) and which may interfere with gel formation. However, salt concentrations up to at least  
143 200 mM do not perturb gel formation. We discuss this point in the last section of the manuscript.  
144 To increase the chances to reach the gel phase, we suggest to add a lag time of 5 min to 10 min  
145 between each addition of HCl aliquots in the pH region between 7.4 and 6.5, when the micelle  
146 to fiber transition occurs. In a standard successful experiment, the total amount of HCl 1 M  
147 added should not increase 50  $\mu$ L for a 1 mL solution at 5 wt%, that is final concentration of  
148 about 50 mM HCl. The final dilution factor, after taking into account the added volume of  
149 NaOH and HCl generally does not exceed 1.03~1.04. Using HCl solution of molarity above  
150 1 M is not recommended due to the sharper pH jumps, which promote the formation of a  
151 precipitate.

152 2) *Use of GDL.* *In-situ* hydrolysis of GDL is known to yield reproducible, stable and  
153 tough hydrogels in low molecular weight gelators. This method was adapted to this system as  
154 follows. A given amount of GDL is weighted in a vial, to which the SLC18:0 solution at basic  
155 pH is added. Mixing is immediately achieved by vortexing for approximately 20 - 30 seconds  
156 and the sample is left at rest (no stirring is applied) with gelation taking place over few hours.  
157 The amounts are approximately 1:0.63 ( $\pm 15\%$ ) = SLC18:0:GDL molar ratio for a SLC18:0  
158 solution at pH ~ 11, and one can also follow the data in Table 1 for convenience. These values  
159 are indicative and we suggest the reader to optimize the amount of GDL on his/her own system.  
160 In fact, the error in the amount of GDL strongly depends on the amount of base introduced in  
161 the solution, that is on the initial pH of the SLC18:0 solution. Specific comments on the  
162 employment of GDL will be given in the last section of the manuscript.

163 **Table 1 – Typical concentration values ( $\pm 15\%$ ) of SLC18:0 and GDL to obtain a homogeneous hydrogel**  
164 **starting from a solution at pH ~11.**

C <sub>SLC18:0</sub> / mg/mL	C <sub>GDL</sub> / mg/mL
10	1.8
17.5	3.1
25	4.5
50	8.9
75	13.4
100	17.8

165

166 3) *Controlled acidification using HCl.*

167 This method was developed in this work in order to prepare reproducible SLC18:0

168 hydrogels using HCl. Manual acidification is replaced by an automated and more controlled  
169 protocol. A given HCl solution (normally 1 M for a 5 wt% SLC18:0 solution) is placed in a  
170 syringe, which is located in a programmable syringe pump. The acidic solution is brought to  
171 the SLC18:0 vial through a thin wall microbore PTFE tube using controlled delivery rates. The  
172 apparatus is shown in Figure S 1. In this work we have spanned the range  $30 < \text{rate} [\mu\text{L}/\text{h}] <$   
173  $6000$ , corresponding to molar rates 30 mM/h and 6 M/h. The SLC18:0 solution should be kept  
174 under stirring ( $\sim 300$  rpm) and pH can be monitored so to stop HCl injection at the desired final  
175 pH value. One should note that the molarity of the HCl solution can vary as long as one adjusts  
176 the acid feeding rate in order to keep the overall molar rate constant and dilution factor low.  
177 For instance, hydrogels with similar properties can be obtained either with a 1 M HCl solution  
178 at a rate of 30  $\mu\text{L}/\text{h}$  (30 mM/h) or with a 0.5 M HCl solution at a rate of 60  $\mu\text{L}/\text{h}$  (30 mM/h).  
179 However using HCl concentrations below 0.5 M is not recommended due to the higher amount  
180 of HCl needed to achieve pH $\sim$ 6, leading to a higher dilution of the final system.

181  
182 *Small Angle X-ray Scattering (SAXS)*. SAXS experiments are performed at 25°C at the  
183 DUBBLE BM26B beamline at the ESRF synchrotron facility (Grenoble, France).<sup>47,48</sup> Samples  
184 have been analysed during the run SC4639 using a beam at 11.93 KeV and a sample-to-detector  
185 distance of 2.10 m. Samples are prepared and inserted in 1 mm quartz tubes. The signal of the  
186 Pilatus 1M 2D detector (172 x 172  $\mu\text{m}$  pixel size), used to record the data, is integrated  
187 azimuthally with PyFAI to obtain the  $I(q)$  vs.  $q$  spectrum ( $q = 4\pi \sin \theta / \lambda$ , where  $2\theta$  is the  
188 scattering angle) after masking systematically wrong pixels and the beam stop shadow. Silver  
189 behenate ( $d_{\text{ref}} = 58.38 \text{ \AA}$ ) is used as SAXS standard to calibrate the  $q$ -scale. Data are not scaled  
190 to absolute intensity.

191  
192 *Rheology*. Viscoelastic measurements were carried out using an Anton Paar MCR 302  
193 rheometer equipped with parallel titanium or stainless steel sandblasted plates (diameter 25  
194 mm). All experiments were conducted at 25 °C and the temperature was controlled by the  
195 stainless steel lower plate, which is the surface of the Peltier system. During experiments, the  
196 measuring geometry was covered with a humidity chamber to minimize water evaporation. To  
197 characterize SLC18:0 hydrogels, strain sweep experiments were first conducted by changing  
198 the shear strain ( $\gamma$ ) from 0.001% to 100% to determine the linear viscoelastic region (LVER).  
199 After loading a new sample, values between  $\gamma = 0.02 - 0.05 \%$  within the LVER were used in  
200 the subsequent angular frequency ( $\omega$ ) sweep from 100 and 0.01  $\text{rad}\cdot\text{s}^{-1}$ . To monitor the gelation



201 kinetic of GDL-induced hydrogels, SLC18:0 solutions were mixed with the appropriate amount  
202 of GDL and the final mixture was vortexed for 20 seconds and immediately loaded on the  
203 bottom plate. Dynamic oscillatory time sweep experiments were performed by applying a  
204 constant oscillation frequency ( $\omega = 6.28 \text{ rad.s}^{-1}$ ) and a shear strain ( $\gamma$ ) within the LVER and data  
205 were collected during 360 minutes. A delay of 3-4 minutes occurs between the moment of  
206 mixing and the beginning of the measurement.

207

208 *<sup>1</sup>H Nuclear Magnetic Resonance (NMR)*: solution NMR was used to follow the kinetics of  
209 micelle-to-fiber phase transition,<sup>49-51</sup> because it is only sensitive to fast-tumbling molecular  
210 species in solution or in micellar environments, while crystalline solids are not detected. Time-  
211 resolved <sup>1</sup>H solution NMR experiments are acquired on a Bruker Avance III 300 spectrometer  
212 using a 5 mm <sup>1</sup>H-X BBFO probe at T= 25°C. Number of transient is 16 with 5 s recycling delay.  
213 Experiments are carried out in D<sub>2</sub>O as follows: a 2.5 wt% concentrated solution of SLC18:0 is  
214 prepared in 99.99% D<sub>2</sub>O at pD ~ 11, using a 5 M solution of NaOD (NaOH powder dispersed  
215 in D<sub>2</sub>O). The solution is split in half and the <sup>1</sup>H NMR spectrum of the first half is recorded. The  
216 second half is added to the corresponding amount of pre-weighted GDL (refer to Table 1)  
217 necessary to obtain a homogeneous hydrogel. The mixture is eventually vortexed and inserted  
218 in a standard 5 mm glass tube. A technical uncompressible delay of about 6 to 7 minutes occurs  
219 between the moment of mixing and the first recorded spectrum. The comparison between the  
220 first spectrum and the solution at basic pH shows no real differences between the two spectra  
221 and for this reason, the first recorded spectrum of the gelation kinetics is used for normalization.  
222 The same experiment is repeated on a solution to which the amount of GDL is doubled, so to  
223 obtain a precipitate instead of a homogeneous hydrogel. Attribution of the <sup>1</sup>H NMR spectrum  
224 of SLC18:0 is provided in detail in ref. <sup>32</sup>.

225 Absolute values of the peak area as a function of time are obtained using the  
226 “integration” and “relaxation” moduli of the Topspin™ 3.5 pl7 version of the software, while  
227 the full width at half maximum (FWHM) profiles have been automatically obtained by using of  
228 DMFit software, available free of charge at the developer’s website.<sup>52,53</sup> We have observed  
229 small phasing problems affecting the peak of H<sub>2</sub>O during the kinetics experiments. Since this  
230 is the most intense peak, poor phasing can affect the baseline in the vicinity of the anomeric  
231 CH between 3 ppm and 4.5 ppm. This unavoidable fact strongly affects the actual value of the  
232 peak area. For this reason, we only calculate the time-resolved evolution of the aliphatic peak  
233 integral contained between 0.5 ppm and 2.5 ppm.

234

235 *Avrami plots.* The Avrami equation is commonly used to determine the nucleation and  
236 growth mechanism of bulk crystals<sup>54,55</sup> and it has been successfully applied to the study of  
237 fibrillar self-assembled gels.<sup>21,22,56</sup> The general form of the Avrami equation is  $X_{cr} = 1 -$   
238  $e^{-kt^n}$ ,  $X_{cr}$  is the volume fraction of the crystalline phase at a given time of the reaction,  $k$  is  
239 the kinetic constant,  $t$  is the time and  $n$  is the type of nucleation (heterogeneous or  
240 instantaneous) and dimensionality of crystal growth, and where  $n$  is commonly contained  
241 between 1 and 4, indicating a 1-D or fiber-like, 2-D or platelet-like and 3-D growth. The Avrami  
242 plot is generally applied in the nucleation and growth phase, so to avoid complex crystallization  
243 effects.<sup>57</sup> Plotting  $\ln\{-\ln[(1 - X_{cr})]\}$  against  $\ln(t)$  gives access to  $n$  (slope) and  $\ln(k)$   
244 (intercept). In this work,  $X_{cr} \equiv X_F$ , where  $X_F$  is the fiber fraction obtained from <sup>1</sup>H NMR  
245 according to  $X_F = (1 - X_M) = (1 - X_A)$ ,<sup>58</sup> where  $X_M$  is the water-soluble micellar fraction,  
246 which is experimentally obtained from the normalized peak area at  $2.5 < \delta/\text{ppm} < 0.5$ , here  
247 referred to obtained as  $X_A$ .

248

249 *Cryogenic Transmission Electron Microscopy (Cryo-TEM).* These experiments were carried  
250 out on an FEI Tecnai 120 twin microscope operating at 120 kV equipped with a Gatan Orius  
251 CCD numeric camera. The sample holder was a Gatan Cryoholder (Gatan 626DH, Gatan).  
252 Digital Micrograph software was used for image acquisition. Cryofixation was done on a  
253 homemade cryofixation device. The solutions were deposited on a glow-discharged holey  
254 carbon coated TEM copper grid (Quantifoil R2/2, Germany). Excess solution was removed and  
255 the grid was immediately plunged into liquid ethane at  $-180$  °C before transferring them into  
256 liquid nitrogen. All grids were kept at liquid nitrogen temperature throughout all  
257 experimentation.

258

## 259 **Results and discussion**

### 260 *SLC18:0 forms hydrogels*

261 The micelle-to-fiber phase transition obtained by the pH-jump method on a diluted  
262 solution (0.5 wt%) of SLC18:0 was studied in detail in previous works by combining cryo-  
263 TEM and pH-resolved *in situ* SAXS.<sup>32,59</sup> In the fiber phase region, we observed that  
264 centrifugation of a stable colloidal solution of SLC18:0 can easily lead to a fiber-rich lower  
265 phase by forced syneresis. This observation suggests that SLC18:0 hydrogels can most likely  
266 be obtained by the direct pH-jump if concentration is high enough, just as observed for  
267 analogous LMWG, where gelation is driven by pH.<sup>18,27,60,61</sup> To test this hypothesis, we prepare  
268 a series of SLC18:0 samples at various concentrations both by manual acidification using HCl  
269 solution (0.5 M or 1 M) and upon addition of GDL to the initial basic solutions at pH 11. The  
270 first method is straightforward but more user-dependent (please, refer to the experimental  
271 section for a note on reproducibility), while the second method is user-independent, it provides  
272 homogeneous SAFIN gels<sup>27</sup> but requires the addition of an extra molecule in close-to-equimolar  
273 amounts (here optimized at 1 SLC18:0 : 0.63 GDL) with respect to SLC18:0, and which could  
274 interfere with the self-assembly process. The rheological properties of a series of SLC18:0  
275 samples prepared at pH 6 and various concentrations using the above mentioned methods are  
276 shown in Figure S 2. Dynamic strain sweep experiments performed on SLC18:0 samples,  
277 prepared both by manual acidification using HCl (Figure S 2a) and upon GDL addition (Figure  
278 S 2b), demonstrate a typical strain softening behavior. At low shear strain values both moduli  
279 exhibit a constant value with  $G' > G''$ , demonstrating the solid-like character of the samples;  
280 upon shear strain increase, both moduli decreases from a given shear strain named as critical  
281 shear strain ( $\gamma_c$ ) which is calculated from the extent of the linear stress ( $\sigma$ ) – strain ( $\gamma$ )  
282 relationship (Figure S 2c). The extent of the linear viscoelastic regime from  $\gamma_c$  is related to  
283 structural changes and gel disruption. At higher shear strain, a  $G' - G''$  crossover is observed  
284 and finally  $G' < G''$ , reflecting the fluidization of the samples, or a gel-to-sol transition. The  
285 angular frequency-dependent storage ( $G'$ ) and loss ( $G''$ ) moduli, measured for all samples both  
286 by manual acidification using HCl (Figure S 2d) and addition of GDL (Figure S 2e), show that  
287  $G'(\omega) > G''(\omega)$ , with no evidence of angular frequency dependence of the storage modulus  
288  $G' \propto \omega^0$ , indicating that samples are gels over the entire angular frequency range.

289 Whichever the acidification method, concentration has a clear impact on the strength of  
290 the hydrogels, where  $2 \cdot 10^{-2} < G'/\text{kPa} < 2$  for manual HCl addition, while  $2 \cdot 10^{-1} < G'/\text{kPa} < 200$   
291 in GDL. However, acidification through GDL systematically provide hydrogels with elastic

292 moduli in the order of two log units higher. This is summarized in profiles showing the  
293 concentration dependency of the gel plateau storage modulus  $G_0(C)$  for both methods of  
294 acidification (Figure 2a). The  $G_0(C)$  behavior is very useful to understand the rheological  
295 behavior of hydrogels and their structural organization, based on theoretical models, originally  
296 established for polymers but extended to fibrillary systems, because self-assembled filaments  
297 can be described as polymers with a significant bending rigidity.<sup>62</sup>  $G_0 \propto AC^n$ , with  $A$  being a  
298 constant and  $n$  an empirical exponent, is a well-known scaling law measured in colloidal and  
299 polymer gels.<sup>63–65</sup> From Figure 2a,  $G_0$  scales linearly with concentration with a slope contained  
300 between 2.0 and 2.4 for both manual HCl acidification and GDL, respectively. This  
301 experimental  $G_0(C)$  behavior is in a good agreement with scaling laws of entangled polymers  
302 in a good solvent and in a semidilute regime with  $n= 2.25$ ,<sup>63</sup> or with  $n = 11/5$ , for entangled  
303 semiflexible biopolymers.<sup>66</sup> Similar values are also found for fibrillary hydrogels composed of  
304 bacterial cellulose<sup>67</sup> and LMWG,<sup>2,18,41,67</sup> but one should also mention that  $n = 5/2$ <sup>66</sup> was also  
305 reported for highly cross-linked semiflexible biopolymer networks. If  $G_0(C)$  indicates that  
306 SLC18:0 samples become stiffer with concentration, they are also more sensitive to  
307 deformation, as highlighted by the decrease of the theoretical critical strain,  $\gamma_c$  with increasing  
308 concentration (Figure S 2f in the supporting information and discussion therein). Such  
309 concentration dependency of  $\gamma_c$  is commonly attributed to the reduction of the mesh size (the  
310 average spacing between fibers) and reduction of the entanglement length (distance between  
311 entanglement points).<sup>66</sup>

312 The normalization of the strain sweep data (Figure S 2g) highlights the strain overshoot  
313 nature of SLC18:0 samples.<sup>68</sup> Such strain hardening overshoot was previously reported for a  
314 wide range of complex fluids like concentrated emulsions<sup>69</sup> or microgels suspensions,<sup>70</sup> but also  
315 for SAFIN without discussing its origin.<sup>71</sup> Depending on the complex fluid, the origin of the  
316 strain overshoot can be attributed to an increase of the effective volume of temporal structures,<sup>72</sup>  
317 to a variation of aggregate size in suspensions<sup>73</sup> or to a rearrangement of clusters<sup>74</sup> during  
318 oscillatory shear deformation.<sup>68</sup> However it's generally assumed that weak strain overshoot is  
319 a result from the balance between the formation and the destruction of the network junctions.<sup>68</sup>  
320 Here, we observe that the intensity of the reduced loss modulus ( $G''/G_0''$ ) does not show a clear  
321 dependence neither on the SLC18:0 concentration nor to the acidification technique (Figure S  
322 2h-i). However, the mere presence of a strain hardening overshoot in this system indicates the  
323 statistically-relevant presence of intermediate-size structures, which under large deformation  
324 will first resist against the imposed deformation, resulting in an increase in  $G''$ , before breaking

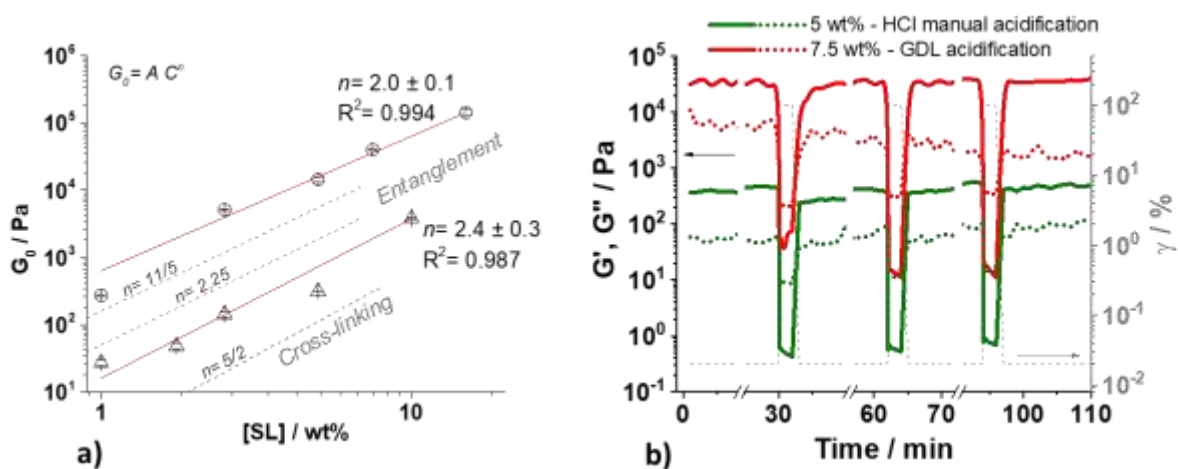
325 up above a given deformation limit, beyond which the SLC180 fibers align with the flow field,  
326 explaining the decrease in  $G''$ . The possible nature of these structures will be discussed by mean  
327 of microscopy tools, later on.

328 Based on the behavior of SLC18:0 samples under small and large strains, we applied  
329 three cycles of step-strain experiments to evaluate the recovery time and mechanical yield of  
330 the hydrogels after applying a large deformation (Figure 2b). During each cycle, samples are  
331 first subjected to a constant strain of 0.02% (in the linear viscoelastic regime,  $0.02\% < \gamma_c$ )  
332 before increasing the strain from 0.1% to 100% during 2 min (large deformation,  $100\% \gg \gamma_c$ )  
333 and the strain is decreased again from 100% to 0.02% for 30 minutes. For both SLC18:0  
334 samples prepared using either HCl or GDL, it was observed that before applying the first large  
335 deformation,  $G'$  is constant and greater than  $G''$ ; however, when a large deformation is applied,  
336  $G'$  becomes lower than  $G''$ , demonstrating the liquid-like behavior of these gel at high strain  
337 values. Immediately after removing the 100% strain, SLC18:0 hydrogels prepared using HCl  
338 and GDL respectively recovered 82% and 77% of their original stiffness (average values after  
339 three cycles). After three cycles, the average complete recovery time is estimated to be ~7 min  
340 and ~3 min for SLC180 hydrogels prepared using HCl and GDL, respectively. The interesting  
341 recovery yield and time (few minutes) highlight the self-healing feature of the SLC18:0  
342 hydrogels.

343 The rheological characterization of SLC18:0 samples prepared both by manual  
344 acidification using HCl and addition of GDL (molar ratio of 1 SLC18:0 : 0.63 GDL)  
345 demonstrate the successful preparation of SLC180 hydrogels with interesting mechanical  
346 properties (stiffness and self-healing properties). We highlight two important points:

- 347 1) The gain in magnitude of the storage modulus  $G'(\omega)$  between the HCl and GDL  
348 approach is close to two orders of magnitude in favour of the GDL approach. This  
349 observation is not surprising and is comparable to what was reported for Fmoc  
350 conjugated peptides,<sup>16,27,28,31</sup> where GDL-driven gelation was implemented to prepare  
351 repeatable homogeneous and strong fibrillar hydrogels. Our results confirm the true  
352 interest in using GDL over manual HCl pH variations also for the SLC18:0 LMWG.
- 353 2) The  $G_0(C)$  behavior of SLC18:0 samples span between theoretical prediction of  
354 hydrogels driven by entanglement, although cross-linking due to tip- and side-branching  
355 should not be excluded: highly cross-linked semiflexible biopolymer networks have  
356 shown an exponent of  $n = 5/2$ , as predicted by the Mackintosh, Käs and Janmey theory.<sup>66</sup>  
357 Moreover, similar exponents were also attributed to cross-linking LMWG-derived  
358 hydrogels.<sup>2,75</sup>

359 If these interesting results class SLC18:0 as a new LMWG, similarly to FMOG  
 360 derivatives and other carbohydrate-based compounds,<sup>76-80</sup> we must highlight a drastic user-  
 361 dependent reproducibility of the hydrogels both when using HCl and non-optimized GDL  
 362 addition. We have in fact experienced many failures, consisting in powder precipitation instead  
 363 of hydrogel formation, while reducing the pH. Considering that all experiments within a given  
 364 method are performed under equal conditions of temperature, initial pH and dilution factors,  
 365 we make the hypothesis that the rate of pH change may have crucial effects in the mechanical  
 366 properties of gel.  
 367



368  
 369 **Figure 2 - a) Evolution of the plateau modulus ( $G_0$ ) with SLC18:0 concentration at pH 6. Gels are prepared**  
 370 **both by manual acidification using HCl 1 M (triangles) and upon GDL addition (circles, molar ratio 1**  
 371 **SLC18 : 0.63 GDL) to basic SLC18:0 solution (initial pH ~11). The dashed lines are theoretical scaling**  
 372 **predictions for entangled semiflexible polymers (De Gennes,  $n= 2.25$ ;<sup>63</sup> Mackintosh et al.,  $n= 11/5$ )<sup>66</sup> and**  
 373 **cross-linked networks (Mackintosh et al.,  $n=5/2$ ).<sup>66</sup> b) Three cycles of step-strain experiments ( $\omega= 6.28$**   
 374 **rad.s<sup>-1</sup>, destructuring at  $\gamma = 100\%$  during 2 min followed by recovery at  $\gamma = 0.02\%$  during 30 min).**  
 375

### 376 *The acidification rate controls the mechanical properties*

377 If manual addition of HCl has long been questioned to provide hydrogels with lower  
 378 elastic moduli<sup>27</sup> and probably being one of the reasons for poor quantitative agreement in terms  
 379 of hydrogel mechanical properties among different authors,<sup>16</sup> the impact of GDL amount on the  
 380 gel properties has equally been questioned.<sup>31</sup> We have ourselves tested several SLC18:0:GDL  
 381 molar ratios and we surprisingly observe that above an optimal amount of GDL, which is  
 382 empirically set at approximately 1:0.63 ( $\pm 15\%$ ), a powdery precipitate is systematically  
 383 observed. Similarly, lower GDL amounts do not promote gelation, because pH remains above  
 384 the micelle-to-fiber phase transition. To prove the direct impact of pH rate change on the

385 hydrogel mechanical properties, we have also prepared several hydrogels replacing the standard  
386 manual HCl 1 M addition (concentration of SLC18:0 was 5 wt%) with a controlled rate by  
387 mean of a syringe pump (apparatus is shown in Figure S 1). We have spanned the pH change  
388 rates over two orders of magnitude, between 30  $\mu\text{L}/\text{h}$  and 6000  $\mu\text{L}/\text{h}$ . Figure 3a and Figure 3b  
389 respectively report the corresponding time-dependent pH profiles, while the mechanical  
390 properties of the final hydrogels prepared using both HCl at different acidification rates and  
391 with different GDL amounts are given in Figure 3c-e.

392 For samples prepared using GDL, the evolution of the pH of a SLC18:0 1 wt% solution  
393 with time at three GDL molar ratios (0.63, 0.94, 1.25) is shown in Figure 3b, while the  
394 corresponding evolutions of  $G'$  are given in Figure 3c. For GDL ratios below 0.94, a  
395 homogeneous hydrogel is systematically obtained, while at 1.25 the solution has practically no  
396 mechanical properties and a powder precipitate is generally observed at the bottom of the vial.  
397 The pH drop profiles with time (Figure 3b) show indeed that the rate of pH change is the same  
398 for all samples below 20 min, that is during the initial hydrolysis of GDL and until pH settles  
399 between 7 and 7.4. Above 20 min, the largest amount of GDL (1.25) induces a faster decay in  
400 pH for a final pH below 5 after 250 min, compared to about 6/6.5 for lower GDL amounts. If  
401 similar differences in terms of pH decay rate have been observed by Adams et al.,<sup>31</sup> they did  
402 not observe an impact on the gel mechanical properties, which was rather affected by the value  
403 of the final pH.<sup>2,30,31</sup> In this work, precipitation occurs as early as 30-40 min after excess of  
404 GDL is added, that is when pH is still sufficiently high (between 6 and 7), in contrast to what  
405 was found with Fmoc-conjugated peptides. If final pH effects are excluded in this system, this  
406 point will be commented in more detail in the last section of this manuscript.

407 For 5 wt% SLC18:0 hydrogels prepared using HCl at different acidification rates, at  
408 6000  $\mu\text{L}/\text{h}$  (black squares), the pH drops below 6 within 1 minute and a powder is immediately  
409 obtained. The corresponding  $G'$  ( $\sim 1$  Pa, Figure 3e) is practically not significant but it is  
410 analogous to the plateau modulus of GDL at 1.25 molar ratio (magenta hexagons, Figure 3c).  
411 At lower HCl addition rates (between 100 and 1000  $\mu\text{L}/\text{h}$ ), the mechanical properties gradually  
412 increase (Figure 3e) up to the kPa domain. The elastic modulus becomes comparable with a 5  
413 wt% gel obtained with manual addition of HCl (Figure 3d), but also with a 1 wt% gel obtained  
414 by using optimal amounts of GDL (black squares, Figure 3c). Very interestingly, for very small  
415 HCl addition rates (30  $\mu\text{L}/\text{h}$ ) the time evolution of pH (diamonds, Figure 3a) matches exactly  
416 the time-dependent pH profiles recorded in the presence of GDL at 0.63 and 0.94 molar ratios  
417 (black and red-segmented lines, Figure 3b) up to 100 min. The elastic modulus of the SLC18:0  
418 5 wt% hydrogel obtained at a HCl addition rate of 30  $\mu\text{L}/\text{h}$  (Figure 3e) is now one order of

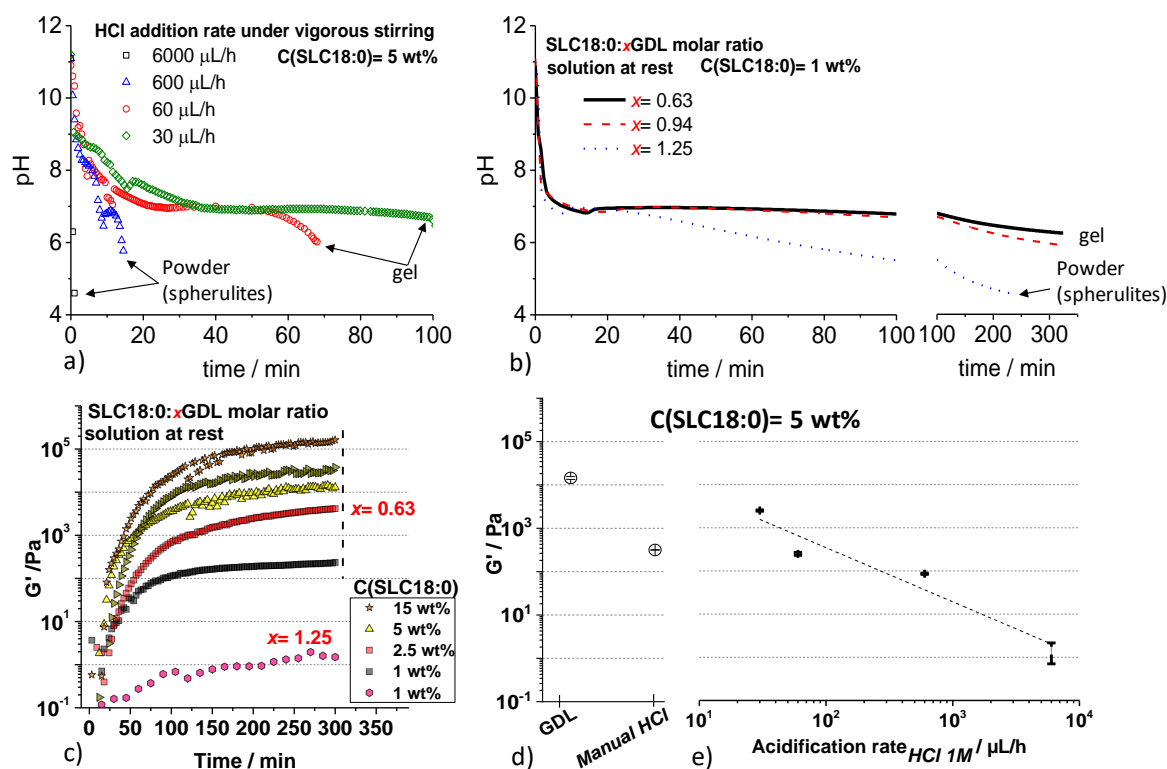
419 magnitude superior if compared to a 5 wt% gel obtained by the manual HCl method (Figure  
420 3d) and only a factor two (linear scale) lower compared to a 5 wt% SLC18:0 hydrogel obtained  
421 by GDL (Figure 3d). In clear, at constant pH (here, 6) and concentration (5 wt%), controlling  
422 the acidification rate below 50  $\mu\text{L}/\text{h}$  generates the same time-dependent evolution of pH  
423 compared to GDL (up to 100 min) and is responsible for a 50-fold improvement in the elastic  
424 modulus compared to manual HCl addition. On the other hand, data in Figure 3d,e also indicate  
425 that manual pH variation, although more difficult to reproduce, can still produce hydrogels with  
426 interesting, yet not optimized, mechanical properties.

427 One can conclude that homogeneous and tough hydrogels with comparable elastic  
428 moduli could be obtained both by GDL and HCl, provided a very low ( $< 30 \mu\text{L}/\text{h}$  for a typical  
429 HCl 1 M used in SLC18:0 at  $C= 5 \text{ wt}\%$ ) acidification rate when employing a HCl solution  
430 (more general considerations on the acidification rates expressed in terms of  $\text{mM}/\text{h}$  are  
431 commented in the last section of the manuscript). Gels are generally formed during the pH-  
432 lowering process but, as expected, hardening occurs after one to two hours after removing the  
433 magnetic stirrer shear. Uncontrolled acidification rates certainly explain part of the  
434 discrepancies in terms of mechanical properties of LMWG hydrogels found in the literature.<sup>16,27</sup>  
435 Moreover, other parameter like stirring (i.e., shearing the sample during hydrogel formation  
436 and fiber growth) during HCl acidification were also suggested to affect the hydrogels  
437 mechanical properties, and which promoted the use of GDL in the past.<sup>29</sup>

438 As a last remark, we highlights that for sufficiently low HCl acidification rates and for  
439 optimum GDL amounts, the pH rises shortly after an initial abrupt drop and before decreasing  
440 again. The length and moment in time of the pH rise varies with the acidification rate (or GDL  
441 amount) but it is systematically observed. Adams et al.,<sup>49,81</sup> as well as other authors<sup>82</sup> reported  
442 the same phenomenon on Fmoc-conjugated peptides acidified with GDL and they attributed it  
443 to the difference between the  $\text{pK}_a$  of the monomer with respect to the apparent  $\text{pK}_a$   
444 corresponding to the self-assembled peptide. This is most likely due to the well-known charge  
445 compensating process, that lies behind the origin of the apparent  $\text{pK}_a$ , a phenomenon often  
446 observed in self-assembled fatty acids. When fatty acids assemble into a crystal or even a  
447 lamellar phase, the surface charge density is initially neutralized by a diffusion of protons from  
448 the bulk solution, which is the origin of the temporary raise in bulk pH.<sup>83-85</sup>

449





450  
 451 **Figure 3 – Time evolution of pH time measured for SLC18:0 solutions ( $V=1\text{ mL}$ ) at a starting pH 11. In a),**  
 452 **the pH of 5 wt% SLC18:0 solutions is lowered under stirring ( $\sim 300\text{ rpm}$ ) using controlled rates of addition**  
 453 **of HCl 1 M. In b), the pH is lowered for a 1 wt% SLC18:0 at pH 11 ( $V=1\text{ mL}$ ) upon vortexing (20 s – 30 s)**  
 454 **with GDL, where  $x$  stands for the GDL molar ratio with respect to one mole of SLC18:0. The solution is left**  
 455 **at rest after vortexing. c) Time evolution of the elastic moduli (data are collected in the linear domain,  $\omega=$**   
 456  **$6.28\text{ rad}\cdot\text{s}^{-1}$ ;  $\gamma=0.02\%$ ) of SLC18:0 solutions at various concentrations upon mixing with GDL. d) Plateau**  
 457 **elastic moduli measured at 5 wt% using the GDL and manual HCl methods. e) Evolution of the plateau**  
 458 **elastic moduli ( $\omega=6.28\text{ rad}\cdot\text{s}^{-1}$ ,  $\gamma=0.02\%$ , each point is averaged over 10 minutes of acquisition) for a series**  
 459 **of 5 wt% SLC18:0 hydrogels prepared from pH 11 with various rates of addition of a 1 M HCl solution.**

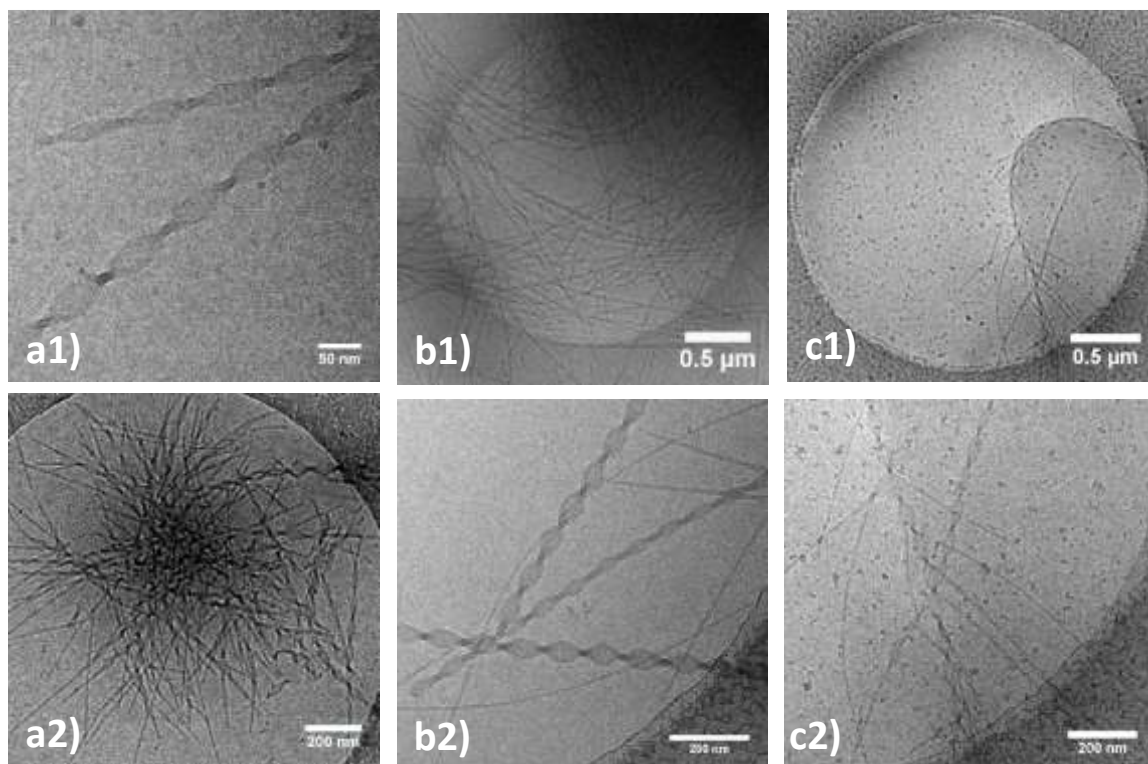
460  
 461 *Supersaturation and spherulite formation depend on the pH change rate. A multiscale analysis.*

462 The data presented above are in contrast, to the best of our knowledge, with the existing  
 463 literature on the mechanistic aspects of pH-driven hydrogels for LMWG (mainly recorded on  
 464 Fmoc-conjugated peptides), and which is based on the following. GDL is preferred to HCl and  
 465 it always gives a homogeneous fibrillar hydrogel. This is shown by Adams<sup>16,27,31</sup> and confirmed  
 466 by micro-rheology data;<sup>82,86</sup> the rate of pH change has little influence on the gel mechanical  
 467 properties, which are rather governed by the final pH.<sup>2,30,31</sup>

468 To better understand the discrepancy between the mechanism of formation of SLC18:0  
 469 hydrogels and Fmoc-conjugated peptides, we investigate the structural and morphological  
 470 properties of the fibers over a broad scale, from the nanometer to the micrometer range,

471 combining SAXS, cryo-TEM and optical microscopy. Data on the kinetics of fiber formation  
472 are also evaluated by  $^1\text{H}$  NMR. It is important to stress that, in order to avoid artifacts, all  
473 experiments have been collected on wet samples and no observation has been performed on  
474 neither air dried nor freeze-dried samples.

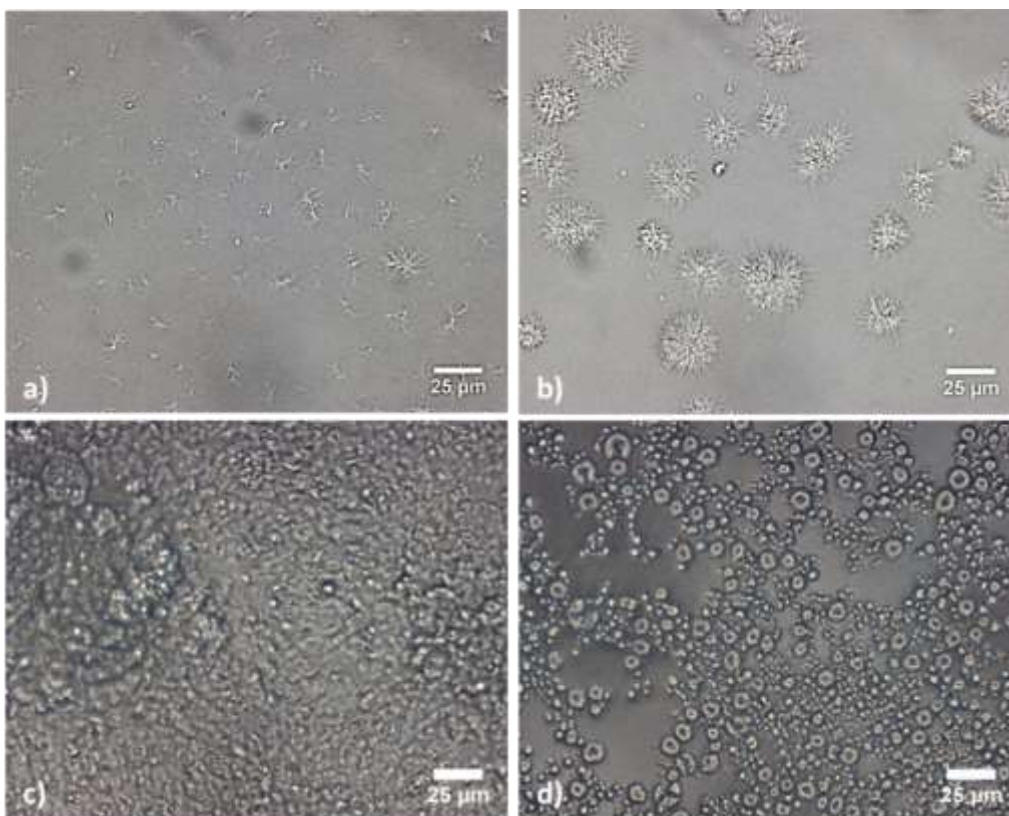
475 The nanoscale structure of the hydrogels prepared both with HCl and GDL has been  
476 studied with SAXS, presented in Figure S 3. The SAXS profiles of hydrogels obtained with  
477 HCl and GDL (Figure S 3a) and with GDL at  $x= 0.63$  (hydrogel) and  $x= 2.52$  (powder  
478 precipitate) (Figure S 3b) are all comparable and they are the typical fingerprint of SLC18:0  
479 twisted ribbons, as described elsewhere.<sup>59,87</sup> All data are characterized by a broad diffraction  
480 peak at  $q= 2.36 \text{ nm}^{-1}$ , indicative of the lipid packing in the ribbon plane, an oscillation at about  
481  $0.75 \text{ nm}^{-1}$ , probably indicating the ribbon form factor, and a strong low- $q$  scattering with no  
482 plateau. The fibrillary and twisted ribbon morphology is confirmed at a larger scale ( $> 100 \text{ nm}$ )  
483 by cryo-TEM experiments presented in Figure 4a1, Figure 4b2 and Figure 4c2 for, respectively,  
484 HCl (5 M, powder), GDL ( $x= 0.63$ , hydrogel) and GDL ( $x= 2.52$ , powder) samples.  
485 Combination of SAXS and cryo-TEM irrefutably show that neither GDL at any amount nor the  
486 pH-change rate have perturbed the formation of twisted ribbons and the packing of SLC18:0  
487 within the ribbons. The poorer mechanical properties observed for excess of GDL and fast pH  
488 change rates must then be explained by differences in the morphology/aggregation at a larger  
489 scale. Cryo-TEM of the powder precipitates obtained either by employing 5 M HCl (Figure  
490 4a2) or GDL  $x= 1.25$  (Figure 4c1, Figure 4c2) shows both spherulitic aggregates (Figure 4a2)  
491 and side branching (Figure 4c1, Figure 4c2). On the contrary, cryo-TEM corresponding to a  
492 stable hydrogel obtained with  $x= 0.63$  GDL shows a homogeneous network of twisted ribbons  
493 with little amount of spherulites and side-branched fibers. One should observe nonetheless that  
494 the fiber cross section is heterogeneous, whichever the approach employed; diameters varying  
495 between 10 nm to 50 nm are not uncommon in none of the samples, as already observed in  
496 more diluted SLC18:0 systems;<sup>32,87</sup> fibers of high cross-sectional uniformity could only be  
497 obtained after dialysis.<sup>87</sup>



498

499 **Figure 4 - a-c) Cryo-TEM images recorded on a series of samples prepared at 0.5 wt% SLC18:0 and**  
 500 **acidified using a1-a2) 5 M HCl (powder precipitate), and SLC18:0:xGDL, with b1-b2)  $x= 0.63$ , c1-c2)  $x=$**   
 501 **1.25.**

502 Further observations at a larger scale using optical microscopy confirm the above  
 503 assumptions. A homogeneous gel (obtained with  $x= 0.63$  GDL) displays a broad fibrillar  
 504 network (SLC18:0 at 1 wt%), where sporadic nucleation centers are not uncommon (Figure 5a).  
 505 Similar results are obtained for the hydrogel prepared at 5 wt% using HCl at a rate of 60  $\mu\text{L}/\text{h}$   
 506 (Figure 5c). In contrast, spherulites strongly characterize those samples that form a precipitate  
 507 in solution, regardless the method of preparation: excess of GDL ( $x= 1.25$ , Figure 5b) and fast  
 508 HCl rates (6000  $\mu\text{L}/\text{h}$ , Figure 5d). Interestingly, the presence of both spherulites and branched  
 509 interconnected fibers is compatible, and it can actually explain, the peculiar strain hardening  
 510 overshoot characterizing the strain sweep data (Figure S 2a,b), and put in evidence in the  
 511 reduced viscous modulus ( $G''/G_0''$ ) as function of the reduced shear strain ( $\gamma/\gamma_c$ ) profiles  
 512 (Figure S 2g,h,i). Rheology data, briefly commented in the mechanical properties section and,  
 513 more extensively, in the Supporting Information, the support the existence of spherulites and  
 514 branched structures from a statistical point of view.

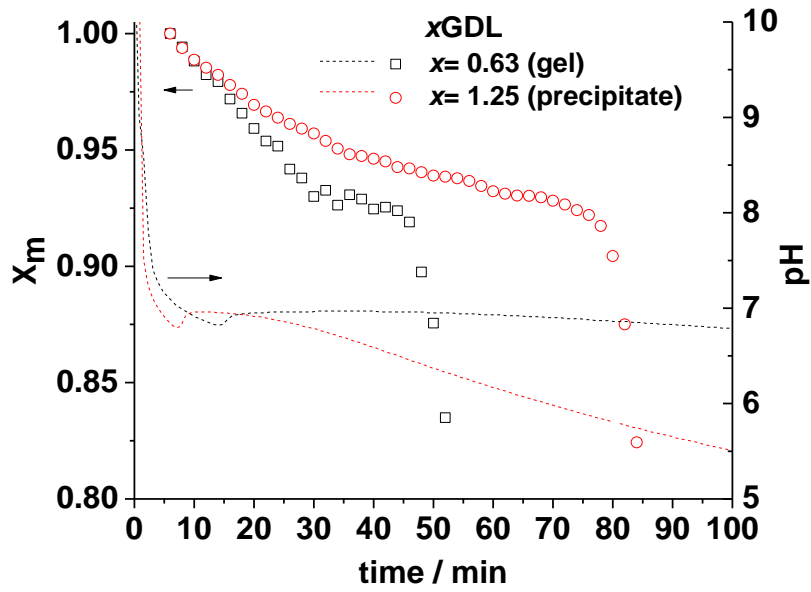


515  
 516 **Figure 5– a,b) Optical microscopy images of SLC18:0 (1 wt%) after  $x$ GDL with a)  $x= 0.63$  and b)  $x= 1.25$ ,**  
 517 **being the SLC18:0: $x$ GDL molar ratio. c,d) Optical microscopy of SLC18:0 (5 wt%) after HCl (1 M) addition**  
 518 **at c) 60  $\mu$ L/h and d) 6000  $\mu$ L/h. For all samples, initial pH  $\sim$ 11 and final pH is contained between 6 and 6.5.**  
 519

520 The kinetics of crystallization can be followed via  $^1\text{H}$  NMR spectroscopy, which is only  
 521 sensitive to the compound in a fast-tumbling (e.g., micellar phase), but not crystalline,  
 522 environment (e.g., fibers). Figure S 4a shows the evolution of the crystalline fraction (as defined  
 523 in the materials and method section),  $X_C$ , of SLC18:0 (2.5 wt%) with time after adding GDL at  
 524  $x= 0.63$  and  $x= 1.25$ , where the former produces a homogeneous gel and the latter a powder  
 525 precipitate. In both cases, the final  $X_C$  is about 0.8, thus excluding the possibility that the poor  
 526 mechanical properties in the  $x= 1.25$  GDL sample depend to a smaller fraction of self-assembled  
 527 fibers. The time evolution of the full width at half maximum (FWHM) shows larger values for  
 528 the gel (up to 35 Hz compared to  $\sim$ 25 Hz for the powder), in agreement with a more  
 529 homogeneous environment, where the mobility of micellar SLC18:0 is further reduced due to  
 530 hydrogel formation. One should note that the discontinuities in both  $X_C$  and FWHM plots are  
 531 most likely artifacts due to problems in a satisfactory baseline subtraction and consequently to  
 532 the signal integration, as explained in the materials and methods section.

533 The multi-scale study shows that the only major difference between two SLC18:0  
 534 samples prepared at the same concentration and temperature but different pH change rates (either





554

555 **Figure 6– Time-evolution of the soluble micellar molar fraction,  $X_m$ , of SLC18:0 (2.5 wt%) in water upon**  
 556 **addition of optimum ( $x= 0.63$ ) and excess ( $x= 1.25$ ) of GDL. The pH change profile is also provided. Initial**  
 557 **pH is ~11.  $x$  is the amount of GDL in the molar ratio SLC18:0: $x$ GDL.**

558

559 Figure 6 demonstrates the link between pH rate change and supersaturation according  
 560 to the assumption that  $\sigma$  is not only temperature but also pH-dependent,  $\sigma(pH)$ . In this case,  
 561 Eq. 1 can be rewritten as in Eq. 2, where dependency on pH is now explicated and dependency  
 562 on temperature is omitted, assuming that all experiments are performed at the same temperature.

563 
$$\sigma(pH) = \frac{C(pH) - C_{eq}(pH)}{C_{eq}(pH)} \quad \text{Eq. 2}$$

564  $C_{eq}(pH)$  is now the pH-dependent equilibrium concentration of SLC18:0; although we do not  
 565 know the exact values,  $C_{eq}(pH)$  is inversely proportional to the concentration of  $[H^+]$  in  
 566 solution (SLC18:0 precipitates in the form of twisted ribbons by lowering the pH).  $C(pH)$ , on  
 567 the contrary, can be estimated through  $^1H$  NMR and its evolution with pH is simply  
 568  $C(pH) = C_{pH11} * X_m(pH)$ , where  $C_{pH11}$  is the SLC18:0 concentration at pH ~11, when it is  
 569 totally dissolved in solution, and  $X_m(pH)$  is the molar fraction of SLC18:0 in a micellar  
 570 environment determined through  $^1H$  NMR. Eq. 2 can then be rewritten and rearranged as a  
 571 function of  $X_m(pH)$ , as follows,

572 
$$\sigma(pH) = X_m(pH) \frac{C_{pH11}}{C_{eq}(pH)} - 1 \quad \text{Eq. 3}$$

573

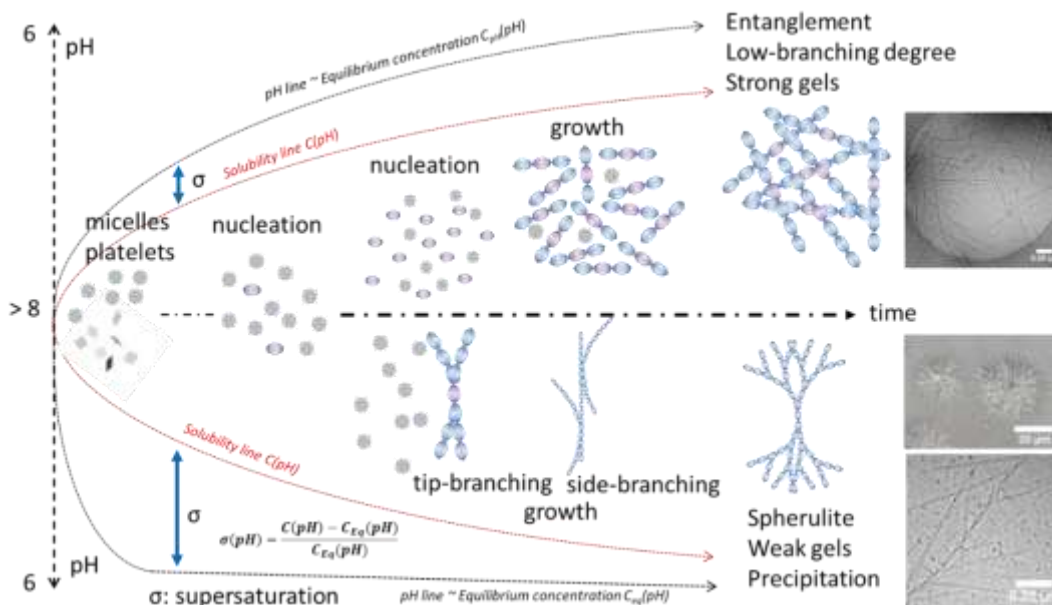
574 When pH decreases,  $\frac{C_{pH11}}{C_{eq}(pH)}$  is always higher than 1 and it is independent of the pH change rate.  
575 On the contrary, even if  $\lim_{pH \rightarrow acid} X_m(pH) \simeq 0$ , the rate at which this event occurs may vary  
576 from system to system.  $\sigma(pH)$  is then maximized when pH is low (small  $C_{eq}(pH)$ ) and when  
577  $\lim_{pH \rightarrow acid} X_m(pH)$  remains close to 1 as long as possible. In other words, if  $X_m(pH)$  is close to  
578 unity all along the decrease in pH, supersaturation is enhanced and branching occurs. This is  
579 experimentally observed for the SLC18:0. Figure 6 shows that  $x=0.63$  GDL after about 70 min,  
580 pH  $\sim 6$  and  $X_m$  has dropped much below 0.8. In this case, one expects small supersaturation and  
581 low branching: at  $x=0.63$  GDL a homogeneous hydrogel is always obtained for any SLC18:0  
582 concentration (Figure 3d, Figure 3c). On the contrary, in excess of GDL,  $X_m(pH)$  decreases at  
583 a much slower rate, while pH drops fast: after 70 min, pH  $\sim 6$  and  $X_m \sim 0.92$ . In this case,  
584 supersaturation and branching are promoted, as verified experimentally (Figure 4c1,c2, Figure  
585 5b,d).

586 The following intriguing question should be answered at this point: why do pH change  
587 rate and supersaturation have such an impact on the self-assembly of SLC18:0, while they do  
588 not on the hydrogel formation of most Fmoc-conjugated peptides, for which GDL concentrations  
589 as high as 2 M are used to form stable hydrogels?<sup>27</sup> To answer this question one could question  
590 both the probability and diffusivity of the acido-base reaction in our system. Literature data  
591 concerning SAFiN hydrogels based on Fmoc-conjugated peptides suggest that in the general  
592  $R - COO^- + H^+ \rightleftharpoons R - COOH$  ( $R$  being a general aliphatic backbone) equilibrium, the  
593 reaction is shifted towards the acid, of which the formation is fast upon acidification and  
594 diffusion is rapid. On the contrary, the data presented in this work on the SAFiN hydrogel  
595 formation of SLC18:0 suggest small reaction probabilities and/or slow diffusion. At a molecular  
596 level, the presence of a micellar phase at basic pH for SLC18:0<sup>32,89</sup> could explain the  
597 discrepancy between SLC18:0 and the literature. Two possible sources of rate-limiting steps  
598 can be identified: 1) low reaction probability of the hydronium ions with the carboxylate groups;  
599 2) slow diffusion of  $R - COOH$  from the micelle to the nucleation site. Although, at present,  
600 none of these hypotheses can be easily verified, we can formulate the following comments.  
601 Reaction rates in micellar solution are well-known to be affected by the presence of the  
602 micelles.<sup>90</sup> In the present system, it could be possible that the reaction probability between  
603 hydronium ions and the carboxylate group in the micelle is not high because the latter does not  
604 necessarily lie at the micelle-water palisade, as in classical head-tail surfactant micelles, but it  
605 could diffuse between the micelle interior and surface. SLC18:0 is a bolaamphiphile and its



606 micellar structure is not as well-defined as the structure of a common head-tail surfactant. We  
 607 have specifically studied the structure of sophorolipid micelles<sup>89,91</sup> and found that the carboxylic  
 608 group could be located within the entire volume of the micelle. In the second hypothesis, two  
 609 scenarios could hold. In the first one, the diffusion rate of a single SLC18:0 molecule after  
 610 protonation is slow compared to the pH change rate; in the second scenario, the micellar  
 611 aggregate is able to retain a critical number of protonated SLC18:0 and above which the micelle  
 612 burst out, thus releasing its entire molecular population, which diffuses immediately towards a  
 613 nucleation site. Unfortunately, we do not dispose of any quantitative data to support these  
 614 scenarios, but we have nonetheless shown that the micelle-to-fiber transition in SLC18:0 occurs  
 615 in a narrow pH range and without any morphological transition between the micelle and the  
 616 fiber, possibly supporting the second scenario.<sup>89</sup> It goes without saying that further  
 617 understanding of the nature of the supersaturation requires further experimental data, but this is  
 618 out of the scope of this work. Nonetheless, Avrami plots (please refer to the materials and  
 619 method section for more information) for the gel and powder samples obtained from <sup>1</sup>H NMR  
 620 data (Figure S 4c) indicate a value for the exponent  $n= 0.45$ , where values of  $n$  below unity,  
 621 although uncommon, are typically found in systems with diffusion-controlled crystallization  
 622 growth and heterogenous nucleation,<sup>56,57,92,93</sup> thus supporting the overall mechanistic  
 623 hypothesis.

624



626 **Figure 7– The pH-dependent mechanism of hydrogelation of SLC18:0 (at room temperature) strongly**  
 627 **depends on the supersaturation level of the solution. For slow pH variations in time (black curve on top),**  
 628 **supersaturation is low and the SAFiN is compatible with a diffusion-limited nucleation and growth of the**  
 629 **fibers, leading to homogenous tough gels. For fast pH variations in time (black curve on the bottom),**



630 **supersaturation is high and the fibrillary network is rich in side branching and spherulites, leading to weak**  
631 **gels or loss of a gel due to precipitation. The red dotted line represents the theoretical solubility line of**  
632 **SLC18:0 with pH.**

633

634 Figure 7 summarizes the main findings of this work; at basic pH, which can be contained  
635 between 8 and 11, SLC18:0 is soluble in water in its ionic form and from previous studies we  
636 know that it forms micelles, although coexisting with a minority of nanoscale platelets (these  
637 can be actually visible in suspension by the eye at pH above 10.5-11).<sup>32,46,59</sup> When pH is reduced  
638 gradually (upper part of scheme in Figure 7 at controlled low rates ( $< \sim 50$  mM/h, please refer  
639 to the last section for more comments on the rate), either using GDL or HCl, both acido-base  
640 reactions at the micelle-water palisade and diffusion of SLC18:0 molecules from the micellar  
641 environment to the nucleation sites are allowed enough time to occur. Growth can then take  
642 place without crystallographic mismatch, because supersaturation is kept at minimum due to  
643 the fact that the molar fraction of soluble solute follows the reduction in the equilibrium  
644 concentration at each pH. A homogeneous fiber network with low degree of branching is  
645 eventually formed and the hydrogel mechanical properties are maximized. On the opposite, if  
646 pH is decreased rapidly, the equilibrium concentration drops too fast with respect to both acido-  
647 base reaction probability and diffusion rate of SLC18:0. In this case, supersaturation is high due  
648 to the large difference between the amount of soluble lipid, still high, and the actual low pH,  
649 which imposes small value of the equilibrium concentration. The high supersaturation  
650 decreases the crystallographic mismatch energy barrier and tip and side branching become then  
651 possible, thus forming spherulites; the mechanical properties of the gel are reduced or even  
652 inexistent, as a powdery precipitate forms. These facts now explain the strong differences in  
653 terms of mechanical properties between the hydrogel obtained by GDL hydrolysis and manual  
654 addition of HCl (Figure S 2), as well as the difficulty to reproduce a hydrogel when HCl is  
655 added manually. Manual addition using HCl solutions of typical molarity between 0.1 M and 1  
656 M is responsible for small, but sensitive, pH jumps, which can be at the origin of supersaturation  
657 phenomena and high degrees of branching. When precipitation due to spherulite formation is  
658 not favored over gelling (most common result), the resulting gel is generally weaker between  
659 one and two orders of magnitude (Figure 3). Using HCl solutions of molarity below 0.1 M  
660 would on the contrary result in an overall dilution of the initial compound, which would also  
661 lead to a weaker gel. In the end, to prepare a reproducible tough hydrogel composed of  
662 SLC18:0, slow ( $< 50$  mM/h) and continuous addition of HCl (generally 0.5 M or 1 M is

663 acceptable) under stirring ( $\leq 300$  rpm), or appropriate amount of GDL (leaving the solution at  
664 rest), should be employed.

665

### 666 *Conceptual and practical considerations*

667 *Effect of charge and relevance of final pH.* Most of the previous literature work states  
668 that the final pH strongly determines the strength and stability of the gel. This effect could be  
669 explained by the neutralization of the negative charges on the fibers. Although side-branching  
670 and spherulite formation could not be explained by such an argument, we have tested the effect  
671 of pH on the stability of the gel for the SLC18:0 system. Electrophoretic mobility experiments  
672 run from pH  $\sim 11$  to pH  $\sim 2$  (Figure S 5a) on a diluted solution (0.25 wt%) of SLC18:0  
673 qualitatively show that negative charges (the exact origin and localization of which are  
674 impossible to determine in this qualitative experiment) are persistent to at least pH 4 and  
675 become negligible below pH 3, below which one should not expect to obtain a stable gel. In  
676 fact, when GDL or controlled addition of HCl solutions are employed, gels are easily obtained  
677 at pH values as low as 2 and they are stable over an “infinite” period of time. At the same time,  
678 spherulite formation, weak gels or precipitation can be observed at pH between 6 and 7, that is  
679 during the nucleation and growth phase and when the system presents negative charges. This is  
680 shown on Figure S 5c,d, where the gel formation is followed in-situ as a function of time for a  
681 SLC18:0 concentration of 5 wt% and using large amounts of GDL. In all cases,  $G' \sim 100$  Pa, a  
682 value that is two orders of magnitude lower than  $G'$  recorded on the same sample, prepared with  
683 the optimized amount of GDL (Figure S 2b). Figure S 5d even shows the loss of all mechanical  
684 properties after about 400 minutes (shrinkage is excluded because the gap is allowed to adjust  
685 setting normal force to zero during measurement). The loss of the properties is simply due to  
686 sedimentation of the spherulites. Sedimentation can actually be observed visually in the  
687 solution. These experiments show that final pH and surface charge are not involved in spherulite  
688 formation and, eventually, precipitation, resulting in the loss of the gel mechanical properties.

689 *Effect of salt.* When spherulites form, one should not expect to have strong gels or even  
690 no gels at all. However, one can increase the pH again above 8 and lower it again by changing  
691 the rate of addition, or adding GDL, for instance. However, starting from basic pH values, and  
692 multiple pH changes in general, generate salt (NaCl in this work), which may have a deleterious  
693 effect on fibrillation, as we have also supposed in a previous work.<sup>94</sup> In a standard experiment  
694 performed for 1 mL solution and SLC18:0 concentration of 5 wt%, one can typically generate  
695 50 mM of NaCl or less, according to the initial pH value. Figure S 5b1 compares the mechanical  
696 properties of two gels prepared under exactly the same conditions (please refer to the

697 Supporting Information for more details). One contains about 20 mM NaCl, simply generated  
698 by the pH change process, and the other one has an additional content of 250 mM of NaCl,  
699 introduced in the solution at basic pH, before the pH change process. The system with high salt  
700 content has slightly worst mechanical properties ( $G' \sim 150$  Pa against  $G' \sim 350$  Pa) and a larger  
701 strain overshoot (Figure S 5b2), suggesting the presence of more spherulitic structures.  
702 However, the effect is far from being impressive and one can consider that both gels still have  
703 mechanical properties in the same order of magnitude. These data suggest that, if needed, one  
704 can regenerate the same gel several times before considering that salt may have an actual effect  
705 on the mechanical properties. Although a thorough study of salt effects are out of the scope of  
706 this work, our experience shows that gels become difficult to reproduce above at least 0.5 M of  
707 NaCl.

708 *GDL against controlled HCl.* Our data show that the gel properties strongly depend on  
709 the kinetics of acid addition, independently of its nature and final pH. To further support this  
710 statement, we have prepared a gel by adding a concentrated solution of gluconic acid to a basic  
711 solution of SLC18:0, where gluconic acid is directly prepared from hydrolyzing GDL in water  
712 overnight. Figure S 5b1,b2 show that the mechanical properties of two gels (concentration of  
713 SLC18:0 is 2.5 wt%, volume is 1 mL), respectively prepared by adding a solution of either HCl  
714 or gluconic acid (both at 0.25 M and added at a rate of 20  $\mu\text{L/h}$ ), are comparable, with  $G'$  ranging  
715 between 200 Pa and 350 Pa. Interestingly, these values are still one order of magnitude smaller  
716 with respect to the use of GDL ( $G' > 10^3$  Pa for SLC18:0 at 2.5 wt%). These data show that: 1)  
717 the nature of the acid is not an important factor; 2) the use of GDL/gluconic acid does not bring  
718 any specific added value to the system, nor it interferes with fibrillation; 3) the rate of GDL  
719 hydrolysis, or the rate of addition of gluconic acid, are, again, the main critical parameters to  
720 control the gel mechanical properties. Of all the experiments that we have performed, it is clear  
721 that use of GDL has systematically provided the strongest gels. However, we stress the fact that  
722 GDL can also induce spherulite formation, weak gels and precipitation. In Table 1, we provide  
723 the optimum amounts of GDL, that we have found for this system. Lower amounts will not  
724 reduce the pH enough while higher amounts provoke a rapid pH transition, favouring spherulite  
725 formation. Nonetheless, the reader should be aware that these values strongly depend on the  
726 initial pH, that is on the amount of base that it is introduced in the system. In fact, reproducibility  
727 of gel with GDL may actually be very poor and should systematically be optimized, because  
728 the amount of initial base may not be strictly identical from one experiment to another. In  
729 addition, hydrolysis rate of GDL is strongly dependent on temperature, which may also limit  
730 the reproducibility of a given experiment. These are certainly the main drawbacks of using

731 GDL. On the contrary, a controlled addition of HCl (or gluconic acid) guaranties a direct control  
732 of the rate and pH at all time, thus ensuring a better reproducibility of the experiment,  
733 independently on the initial pH value.

734 If having a good control of the addition rate of the acid guarantees a more reproducible  
735 result from one user to another, gels prepared through GDL still seem to have better mechanical  
736 properties. Although GDL hydrolysis is not homogeneous in time, one can qualitatively  
737 evaluate an equivalent corresponding acidification rate. For practical reasons, acidification rates  
738 throughout this work are reported in  $\mu\text{L}/\text{h}$ , but using  $\text{mM}/\text{h}$  units will help comparing  
739 acidifications rates with GDL and HCl. For a typical SLC18:0 concentration of 5 wt% in 1 mL  
740 at pH 11, we have employed a 50 mM solution of GDL (Table 1). If the experiment is run over  
741 300 min, one can estimate an average hydrolysis rate of 10 mM/h. Interestingly, if the same  
742 system is acidified with a 1 M HCl solution added at 30  $\mu\text{L}/\text{h}$  (Figure 3e), the rate is 30 mM/h,  
743 that is three times faster, resulting in a weaker gel. These considerations reinforce the idea that  
744 the hydrolysis rate is the actual key to control the mechanical properties of the gel.

745 *Other factors.* It may not be excluded that other factors may play a key role and are  
746 worth exploring in the future: 1) constancy of the acidification rate; 2) initial pH; 3) stirring; 4)  
747 volumes; 5) nucleation centers. The acidification profiles of GDL and HCl are not the same in  
748 the beginning of the acidification curve (Figure 3a,b). At the moment, it is not clear whether or  
749 not the rate of pH change before fibrillation has any significant impact, nor it is clear whether  
750 or not the initial pH plays a role. According to our experience, good quality gels can be obtained  
751 starting when initial pH is 11 (data in this work) or 9. We have also obtained strong gels both  
752 when acidification rate is either constant or not. However, these qualitative results do not mean  
753 that these parameters may not have an effect on branching, and consequently on gel strength.  
754 Stirring, only employed here upon HCl acidification, may also have an important effect. We  
755 have experienced good gels both under strong ( $> 500$  rpm) and mild ( $< 200$  rpm) stirring  
756 conditions, but it may not be excluded that the better mechanical properties of the GDL-  
757 acidified systems are related to its steady state. In this case, when employing HCl, one could  
758 prefer mild stirring conditions, which, however, may not guarantee satisfactory  
759 homogenization. Adapting the size of the stirrer to the volume of the solution may also be an  
760 important parameter to explore. Finally, the entire process described in this work is governed  
761 by heterogenous nucleation phenomena, whereas the presence of a substrate lowers the energy  
762 barrier. It may not be excluded that small heterogeneities may favor spherulite nucleation and  
763 growth. Spurious use of ultrasounds can be possible during the nucleation phase to help dissolve  
764 the nuclei before lowering the pH.

765

## 766 **Conclusion**

767 In this work we explore the pH-driven hydrogel properties of stearic acid sophorolipid,  
768 a microbial glycolipid. This compound is known to undergo a micelle-to-twisted ribbon phase  
769 transition around pH 7.4 and we show here that above 1 wt% it is possible to form a self-  
770 assembled fibrillary network (SAFiN) hydrogel. At a first glance, this system behaves as  
771 fluorenyl-9-methoxycarbonyl (Fmoc) amino acid derivatives, which form hydrogels below a  
772 given pH. In particular, we show that use of internal acidification using the hydrolysis of  
773 glucono- $\delta$ -lactone (GDL) provides a homogenous and stronger hydrogel than a more classical  
774 manual pH variation approach using HCl. Oscillatory rheology experiments show that  
775 acidification through GDL provides elastic moduli in the range between 10 kPa and 100 kPa,  
776 while after using HCl the elastic moduli are rarely higher than 1 kPa. These results corroborate  
777 the data recorded on other pH-responsive hydrogels prepared using Fmoc derivatives.  
778 However, the admitted mechanistic behavior in pH-responsive hydrogels is that the final pH  
779 governs the gel mechanical properties, which is not what we find in this work.

780 In the second part of the paper we demonstrate that mechanical properties of SLC180  
781 hydrogel do not actually depend on the acidification method itself but on the rate of  
782 acidification, may it occur through HCl addition, provided a strict control over the addition of  
783 HCl to the solution, or GDL hydrolysis. In contrast to what is generally known, both HCl and  
784 GDL can induce a phase separation observed through precipitation of spherulites in the solution.  
785 If SAXS experiments show that whichever the method of preparation, SLC18:0 always  
786 nucleates into self-assembled fibers below neutral pH, cryo-TEM and optical microscopy  
787 experiments allow to associate side branching and spherulite formation of fast HCl acidification  
788 rates or excess of GDL. Rheology shows, on the contrary, that hydrogels with similar  
789 mechanical properties can be prepared with low HCl acidification rates or optimal GDL  
790 amount. Solution NMR spectroscopy performed on two systems, one containing excess  
791 (leading to precipitation) and the other an optimal amount (leading to gel) of GDL, reveals an  
792 important mismatch between the expected equilibrium and measured SLC18:0 concentrations  
793 as a function of pH when excess of GDL is employed. This experiment proves the existence of  
794 supersaturation when pH changes too fast. Supersaturation is known to decrease the  
795 crystallographic mismatch nucleation energy, a necessary and sufficient condition to observe  
796 side branching and spherulite formation in SAFiN prepared with low molecular weight gelators.  
797 In clear, slow acidification rates promote strong SLC18:0 hydrogels with low, or no, degree of  
798 branching, while high acidification rates promote highly branched fibers forming weak gels, or

799 no gels at all. Although the origin of this phenomenon is still not clear, we think that the micellar  
800 environment in the pH region prior to nucleation and growth of the fibers establishes a limited  
801 process, slowing down the SLC18:0 molecular diffusion from the micelles to the nucleating  
802 fibers. Additional experiments are needed to better understand this phenomenon.

803

#### 804 **Acknowledgements**

805 Research leading to these results received funding from the European Community's Seventh  
806 Framework Programme (FP7/2007–2013) under Grant Agreement No. Biosurfing/289219.  
807 This work also received financial support by the European Synchrotron Radiation Facility  
808 (ESRF), Grenoble, France, under the experiment number SC 4778. Mr. Abdoul Aziz Ba  
809 (Sorbonne Université, Paris, France) and Mrs Chloé Seyrig (Sorbonne Université, Paris,  
810 France) are acknowledged for their experimental assistance. Dr. Thibaut Divoux (CNRS, MIT)  
811 is acknowledged for helpful discussion on rheology.

812

813 **Supporting Information.** Figure S 1 illustrates the typical setup employed for controlled  
814 acidification. Figure S 2 shows the rheological properties of SLC18:0 hydrogels. Figure S 3  
815 shows Small Angle X-ray Scattering experiments. Figure S 4 reports the kinetic experiments  
816 (mmicelles molar fraction, FWHM and Avrami plots) performed through <sup>1</sup>H solution NMR.  
817 Figure S 5 combines electrophoretic mobility experiments and complementary rheology  
818 analyses. This material is available free of charge via the internet at <http://pubs.acs.org>

819 **References**

- 820 (1) Okesola, B. O.; Smith, D. K. Applying Low-Molecular Weight Supramolecular  
821 Gelators in an Environmental Setting-Self-Assembled Gels as Smart Materials for  
822 Pollutant Removal. *Chem. Soc. Rev.* **2016**, *45*, 4226–4251.
- 823 (2) Colquhoun, C.; Draper, E. R.; Schweins, R.; Marcello, M.; Vadukul, D.; Serpell, L. C.;  
824 Adams, D. J. Controlling the Network Type in Self-Assembled Dipeptide Hydrogels.  
825 *Soft Matter* **2017**, *13*, 1914–1919.
- 826 (3) Venkatesh, V.; Mishra, N. K.; Romero-Canelón, I.; Vernooij, R. R.; Shi, H.;  
827 Coverdale, J. P. C.; Habtemariam, A.; Verma, S.; Sadler, P. J. Supramolecular  
828 Photoactivatable Anticancer Hydrogels. *J. Am. Chem. Soc.* **2017**, *139*, 5656–5659.
- 829 (4) Ramin, M. A.; Latxague, L.; Sindhu, K. R.; Chassande, O.; Barthélémy, P. Low  
830 Molecular Weight Hydrogels Derived from Urea Based-Bolaamphiphiles as New  
831 Injectable Biomaterials. *Biomaterials* **2017**, *145*, 72–80.
- 832 (5) Huang, G.; Li, F.; Zhao, X.; Ma, Y.; Li, Y.; Lin, M.; Jin, G.; Lu, T. J.; Genin, G. M.;  
833 Xu, F. Functional and Biomimetic Materials for Engineering of the Three-Dimensional  
834 Cell Microenvironment. *Chem. Rev.* **2017**, *117*, 12764–12850.
- 835 (6) Nolan, M. C.; Fuentes Caparrós, A. M.; Dietrich, B.; Barrow, M.; Cross, E. R.; Bleuel,  
836 M.; King, S. M.; Adams, D. J. Optimising Low Molecular Weight Hydrogels for  
837 Automated 3D Printing. *Soft Matter* **2017**, *13*, 8426–8432.
- 838 (7) Frith, W. J. Self-Assembly of Small Peptide Amphiphiles, the Structures Formed and  
839 Their Applications. (a Foods and Home and Personal Care Perspective). *Philos. Trans.*  
840 *R. Soc. A Math. Phys. Eng. Sci.* **2016**, *374*, 20150138.
- 841 (8) Stubenrauch, C.; Gießelmann, F. Gelled Complex Fluids: Combining Unique  
842 Structures with Mechanical Stability. *Angew. Chemie - Int. Ed.* **2016**, *55*, 3268–3275.
- 843 (9) Sydney Gladman, A.; Matsumoto, E. A.; Nuzzo, R. G.; Mahadevan, L.; Lewis, J. A.  
844 Biomimetic 4D Printing. *Nat. Mater.* **2016**, *15*, 413–418.
- 845 (10) Draper, E. R.; Adams, D. J. Low-Molecular-Weight Gels: The State of the Art. *Chem*  
846 **2017**, *3*, 390–410.
- 847 (11) Du, X.; Zhou, J.; Shi, J.; Xu, B. Supramolecular Hydrogelators and Hydrogels: From  
848 Soft Matter to Molecular Biomaterials. *Chem. Rev.* **2015**, *115*, 13165–13307.
- 849 (12) Qiao, Y.; Lin, Y.; Yang, Z.; Chen, H.; Zhang, S.; Yan, Y.; Huang, J. Unique  
850 Temperature-Dependent Supramolecular Self-Assembly: From Hierarchical 1D  
851 Nanostructures to Super Hydrogel. *J. Phys. Chem. B* **2010**, *114*, 11725–11730.
- 852 (13) Jayawarna, V.; Ali, M.; Jowitt, T. A.; Miller, A. F.; Saiani, A.; Gough, J. E.; Ulijn, R.

- 853 V. Nanostructured Hydrogels for Three-Dimensional Cell Culture Through Self-  
854 Assembly of Fluorenylmethoxycarbonyl–Dipeptides. *Adv. Mater.* **2006**, *18*, 611–614.
- 855 (14) Ozbas, B.; Kretsinger, J.; Rajagopal, K.; Schneider, J. P.; Pochan, D. J. Salt-Triggered  
856 Peptide Folding and Consequent Self-Assembly into Hydrogels with Tunable Modulus.  
857 *Macromolecules* **2004**, *37*, 7331–7337.
- 858 (15) He, H.; Wang, H.; Zhou, N.; Yang, D.; Xu, B. Branched Peptides for Enzymatic  
859 Supramolecular Hydrogelation. *Chem. Commun.* **2018**, *54*, 86–89.
- 860 (16) Raeburn, J.; Cardoso, A. Z.; Adams, D. J. The Importance of the Self-Assembly  
861 Process to Control Mechanical Properties of Low Molecular Weight Hydrogels. *Chem.*  
862 *Soc. Rev.* **2013**, *42*, 5143–5156.
- 863 (17) Jung, J. H.; Rim, J. A.; Han, W. S.; Lee, S. J.; Lee, Y. J.; Cho, E. J.; Kim, J. S.; Ji, Q.;  
864 Shimizu, T. Hydrogel Behavior of a Sugar-Based Gelator by Introduction of an  
865 Unsaturated Moiety as a Hydrophobic Group. *Org. Biomol. Chem.* **2006**, *4*, 2033–  
866 2038.
- 867 (18) Greenfield, M. A.; Hoffman, J. R.; De La Cruz, M. O.; Stupp, S. I. Tunable Mechanics  
868 of Peptide Nanofiber Gels. *Langmuir* **2010**, *26*, 3641–3647.
- 869 (19) Clemente, M. J.; Fitremann, J.; Mauzac, M.; Serrano, J. L.; Oriol, L. Synthesis and  
870 Characterization of Maltose-Based Amphiphiles as Supramolecular Hydrogelators.  
871 *Langmuir* **2011**, *27*, 15236–15247.
- 872 (20) Jung, J. H.; John, G.; Masuda, M.; Yoshida, K.; Shinkai, S.; Shimizu, T. Self-Assembly  
873 of a Sugar-Based Gelator in Water: Its Remarkable Diversity in Gelation Ability and  
874 Aggregate Structure. *Langmuir* **2001**, *17*, 7229–7232.
- 875 (21) Liu, X. Y.; Sawant, P. D. Mechanism of the Formation of Self-Organized  
876 Microstructures in Soft Functional Materials. *Adv. Mater.* **2002**, *14*, 421–426.
- 877 (22) Liu, X. Y.; Sawant, P. D. Formation Kinetics of Fractal Nanofiber Networks in  
878 Organogels. *Appl. Phys. Lett.* **2001**, *79*, 3518–3520.
- 879 (23) Wang, R.; Liu, X.-Y.; Xiong, J.; Li, J. Real-Time Observation of Fiber Network  
880 Formation in Molecular Organel: Supersaturation-Dependent Microstructure and Its  
881 Related Rheological Property. *J. Phys. Chem. B.* **2006**, *110*, 7275.
- 882 (24) Yu, R.; Lin, N.; Yu, W.; Liu, X. Y. Crystal Networks in Supramolecular Gels:  
883 Formation Kinetics and Mesoscopic Engineering Principles. *CrystEngComm* **2015**, *17*,  
884 7986–8010.
- 885 (25) Draper, E. R.; Mears, L. L. E.; Castilla, A. M.; King, S. M.; McDonald, T. O.; Akhtar,  
886 R.; Adams, D. J. Using the Hydrolysis of Anhydrides to Control Gel Properties and



- 887 Homogeneity in PH-Triggered Gelation. *RSC Adv.* **2015**, *5*, 95369–95378.
- 888 (26) Raeburn, J.; McDonald, T. O.; Adams, D. J. Dipeptide Hydrogelation Triggered via  
889 Ultraviolet Light. *Chem. Commun.* **2012**, *48*, 9355–9357.
- 890 (27) Adams, D. J.; Butler, M. F.; Frith, W. J.; Kirkland, M.; Mullen, L.; Sanderson, P. A  
891 New Method for Maintaining Homogeneity during Liquid-Hydrogel Transitions Using  
892 Low Molecular Weight Hydrogelators. *Soft Matter* **2009**, *5*, 1856–1862.
- 893 (28) Wang, H.; Yang, Z.; Adams, D. J. Controlling Peptide-Based Hydrogelation. *Mater.*  
894 *Today* **2012**, *15*, 500–507.
- 895 (29) Helen, W.; De Leonardis, P.; Ulijn, R. V.; Gough, J.; Tirelli, N. Mechanosensitive  
896 Peptide Gelation: Mode of Agitation Controls Mechanical Properties and Nano-Scale  
897 Morphology. *Soft Matter* **2011**, *7*, 1732–1740.
- 898 (30) Johnson, E. K.; Adams, D. J.; Cameron, P. J. Directed Self-Assembly of Dipeptides to  
899 Form Ultrathin Hydrogel Membranes. *J. Am. Chem. Soc.* **2010**, *132*, 5130–5136.
- 900 (31) Chen, L.; Morris, K.; Laybourn, A.; Elias, D.; Hicks, M. R.; Rodger, A.; Serpell, L.;  
901 Adams, D. J. Self-Assembly Mechanism for a Naphthalene-Dipeptide Leading to  
902 Hydrogelation. *Langmuir* **2010**, *26*, 5232–5242.
- 903 (32) Cuvier, A. S.; Berton, J.; Stevens, C. V; Fadda, G. C.; Babonneau, F.; Van Bogaert, I.  
904 N. A.; Soetaert, W.; Pehau-Arnaudet, G.; Baccile, N. PH-Triggered Formation of  
905 Nanoribbons from Yeast-Derived Glycolipid Biosurfactants. *Soft Matter* **2014**, *10*,  
906 3950–3959.
- 907 (33) Van Bogaert, I. N. A.; Saerens, K.; De Muynck, C.; Develter, D.; Soetaert, W.;  
908 Vandamme, E. J. Microbial Production and Application of Sophorolipids. *Appl.*  
909 *Microbiol. Biotechnol.* **2007**, *76*, 23–34.
- 910 (34) Marchant, R.; Banat, I. M. Microbial Biosurfactants: Challenges and Opportunities for  
911 Future Exploitation. *Trends Biotechnol.* **2012**, *30*, 558–565.
- 912 (35) Dhasaiyan, P.; Banerjee, A.; Visaveliya, N.; Prasad, B. L. V. Influence of the  
913 Sophorolipid Molecular Geometry on Their Self-Assembled Structures. *Chem. Asian J.*  
914 **2013**, *8*, 369–372.
- 915 (36) Dhasaiyan, P.; Prasad, B. L. V. Self-Assembly of Bolaamphiphilic Molecules. *Chem.*  
916 *Rec.* **2017**, *17*, 597–610.
- 917 (37) Zhou, S.; Xu, C.; Wang, J.; Gao, W.; Akhverdiyeva, R.; Shah, V.; Gross, R.  
918 Supramolecular Assemblies of a Naturally Derived Sophorolipid. *Langmuir* **2004**, *20*,  
919 7926–7932.
- 920 (38) Roelants, S. L. K. W.; Renterghem, L. Van; Maes, K.; Everaert, B.; Redant, E.;

- 921 Vanlerberghe, B.; Demaeseneire, S.; Soetaert, W. Taking Biosurfactants from the Lab  
922 to the Market: Hurdles and How to Take Them by Applying an Integrated Process  
923 Design Approach. In *Microbial Biosurfactants and their Environmental and Industrial*  
924 *Applications*; Banat, I. M., Thavasi, R., Eds.; CRC Press, 2018.
- 925 (39) Imura, T.; Kawamura, D.; Ishibashi, Y.; Morita, T.; Sato, S.; Fukuoka, T.; Kikkawa,  
926 Y.; Kitamoto, D. Low Molecular Weight Gelators Based on Biosurfactants, Cellobiose  
927 Lipids by *Cryptococcus Humicola*. *J. Oleo Sci.* **2012**, *61*, 659–664.
- 928 (40) Imura, T.; Yamamoto, S.; Yamashita, C.; Taira, T.; Minamikawa, H.; Morita, T.;  
929 Kitamoto, D. Aqueous Gel Formation from Sodium Salts of Cellobiose Lipids. *J. Oleo*  
930 *Sci.* **2014**, *63*, 1005–1010.
- 931 (41) Baccile, N.; Renterghem, L. Van; Griel, P. Le; Ducouret, G.; Brennich, M.; Cristiglio,  
932 V.; Roelants, S. L. K. W.; Soetaert, W. Bio-Based Glyco-Bolaamphiphile Forms a  
933 Temperature-Responsive Hydrogel with Tunable Elastic Properties. *Soft Matter* **2018**,  
934 *14*, 7859–7872.
- 935 (42) Wang, R. Y.; Liu, X. Y.; Narayanan, J.; Xiong, J. Y.; Li, J. L. Architecture of Fiber  
936 Network: From Understanding to Engineering of Molecular Gels. *J. Phys. Chem. B*  
937 **2006**, *110*, 25797–25802.
- 938 (43) Liu, X. Y. Gelation with Small Molecules: From Formation Mechanism to  
939 NanostructureArchitecture. *Top. Curr. Chem.* **2005**, *256*, 1–37.
- 940 (44) Wang, R.; Liu, X.-Y.; Xiong, J.; Li, J. Real-Time Observation of Fiber Network  
941 Formation in Molecular Organel: Supersaturation-Dependent Microstructure and Its  
942 Related Rheological Property. *J. Phys. Chem. B.* **2006**, *110*, 7275.
- 943 (45) Baccile, N.; Cuvier, A.-S.; Valotteau, C.; Van Bogaert, I. N. A. Practical Methods to  
944 Reduce Impurities for Gram-Scale Amounts of Acidic Sophorolipid Biosurfactants.  
945 *Eur. J. Lipid Sci. Technol.* **2013**, *115*, 1404–1412.
- 946 (46) Cuvier, A. S.; Babonneau, F.; Berton, J.; Stevens, C. V.; Fadda, G. C.; Péhau-  
947 Arnaudet, G.; Le Griel, P.; Prévost, S.; Perez, J.; Baccile, N. Nanoscale Platelet  
948 Formation by Monounsaturated and Saturated Sophorolipids under Basic PH  
949 Conditions. *Chem. - A Eur. J.* **2015**, *21*, 19265–19277.
- 950 (47) Bras, W.; Dolbnya, I. P.; Detollenaere, D.; van Tol, R.; Malfois, M.; Greaves, G. N.;  
951 Ryan, A. J.; Heeley, E. Recent Experiments on a Small-Angle/Wide-Angle X-Ray  
952 Scattering Beam Line at the ESRF. *J. Appl. Crystallogr.* **2003**, *36*, 791–794.
- 953 (48) Portale, G.; Cavallo, D.; Alfonso, G. C.; Hermida-Merino, D.; van Drongelen, M.;  
954 Balzano, L.; Peters, G. W. M.; Goossens, J. G. P.; Bras, W. Polymer Crystallization

- 955 Studies under Processing-Relevant Conditions at the SAXS/WAXS DUBBLE  
956 Beamline at the ESRF. *J. Appl. Crystallogr.* **2013**, *46*, 1681–1689.
- 957 (49) Wallace, M.; Iggo, J. A.; Adams, D. J. Using Solution State NMR Spectroscopy to  
958 Probe NMR Invisible Gelators. *Soft Matter* **2015**, *11*, 7739–7747.
- 959 (50) Fuhrhop, J. H.; Svenson, S.; Boettcher, C.; Rössler, E.; Vieth, H. M. Long-Lived  
960 Micellar N-Alkylaldonamide Fiber Gels. Solid-State NMR and Electron Microscopic  
961 Studies. *J. Am. Chem. Soc.* **1990**, *112*, 4307–4312.
- 962 (51) Frkanec, L.; Jokić, M.; Makarević, J.; Wolsperger, K.; Žinić, M. Bis(PheOH) Maleic  
963 Acid Amide-Fumaric Acid Amide Photoisomerization Induces Microsphere-to-Gel  
964 Fiber Morphological Transition: The Photoinduced Gelation System. *J. Am. Chem.*  
965 *Soc.* **2002**, *124*, 9716–9717.
- 966 (52) <http://nmr.cemhti.cnrs-orleans.fr/dmfit>. DMFit <http://nmr.cemhti.cnrs-orleans.fr/dmfit>.
- 967 (53) Massiot, D.; Fayon, F.; Capron, M.; King, I.; Calvé, S. Le; Alonso, B.; Durand, J. O.;  
968 Bujoli, B.; Gan, Z.; Hoatson, G. Modelling One and Two-Dimensional Solid-State  
969 NMR Spectra. *Magn. Reson. Chem.* **2002**, *40*, 70–76.
- 970 (54) Avrami, M. Kinetics of Phase Change. I General Theory. *J. Chem. Phys.* **1939**, *7*,  
971 1103–1112.
- 972 (55) Avrami, M. Granulation, Phase Change, and Microstructure Kinetics of Phase Change.  
973 III. *J. Chem. Phys.* **1941**, *9*, 177–184.
- 974 (56) Terech, P. Kinetics of Aggregation in a Steroid Derivative/Cyclohexane Gelifying  
975 System. *J. Colloid Interface Sci.* **1985**, *107*, 244–255.
- 976 (57) Lopes-da-Silva, J. A.; Coutinho, J. A. P. Analysis of the Isothermal Structure  
977 Development in Waxy Crude Oils under Quiescent Conditions. *Energy and Fuels*  
978 **2007**, *21*, 3612–3617.
- 979 (58) Feio, G.; Cohen-Addad, J. P. NMR Approach to the Kinetics of Polymer  
980 Crystallization. 1. Cis-1,4-Polybutadiene. *J. Polym. Sci. Part B Polym. Phys.* **1988**, *26*,  
981 389–412.
- 982 (59) Baccile, N.; Cuvier, A. S.; Prévost, S.; Stevens, C. V.; Delbeke, E.; Berton, J.; Soetaert,  
983 W.; Van Bogaert, I. N. A.; Roelants, S. Self-Assembly Mechanism of PH-Responsive  
984 Glycolipids: Micelles, Fibers, Vesicles, and Bilayers. *Langmuir* **2016**, *32*, 10881–  
985 10894.
- 986 (60) Tang, C.; Smith, A. M.; Collins, R. F.; Ulijn, R. V.; Saiani, A. Fmoc-Diphenylalanine  
987 Self-Assembly Mechanism Induces Apparent PKaShifts. *Langmuir* **2009**, *25*, 9447–  
988 9453.

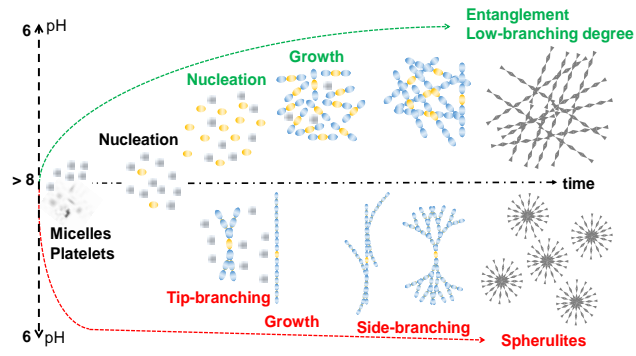
- 989 (61) Tang, C.; Ulijn, R. V.; Saiani, A. Effect of Glycine Substitution on Fmoc-  
990 Diphenylalanine Self-Assembly and Gelation Properties. *Langmuir* **2011**, *27*, 14438–  
991 14449.
- 992 (62) Kierfeld, J.; Baczynski, K.; Gutjahr, P.; Lipowsky, R. *Semiflexible Polymers and*  
993 *Filaments: From Variational Problems to Fluctuations*; 2008; Vol. 1002.
- 994 (63) de Gennes, P.-G. Dynamics of Entangled Polymer Solutions. I. The Rouse Model.  
995 *Macromolecules* **1976**, *9*, 587–593.
- 996 (64) de Rooij, R.; van den Ende, D.; Duits, M. H. G.; Mellema, J. Elasticity of Weakly  
997 Aggregating Polystyrene Latex Dispersions. *Phys. Rev. E* **1994**, *49*, 3038–3049.
- 998 (65) Flory, P. J. *Principles of Polymer Chemistry*; Cornell University Press: Ithaca, NY,  
999 NY, 1953.
- 1000 (66) MacKintosh, F. C.; Käs, J.; Janmey, P. A. Elasticity of Semiflexible Biopolymer  
1001 Networks. *Phys. Rev. Lett.* **1995**, *75*, 4425–4428.
- 1002 (67) Chen, S. Q.; Lopez-Sanchez, P.; Wang, D.; Mikkelsen, D.; Gidley, M. J. Mechanical  
1003 Properties of Bacterial Cellulose Synthesised by Diverse Strains of the Genus  
1004 *Komagataeibacter*. *Food Hydrocoll.* **2018**, *81*, 87–95.
- 1005 (68) Hyun, K.; Wilhelm, M.; Klein, C. O.; Cho, K. S.; Nam, J. G.; Ahn, K. H.; Lee, S. J.;  
1006 Ewoldt, R. H.; McKinley, G. H. A Review of Nonlinear Oscillatory Shear Tests:  
1007 Analysis and Application of Large Amplitude Oscillatory Shear (LAOS). *Prog. Polym.*  
1008 *Sci.* **2011**, *36*, 1697–1753.
- 1009 (69) Mason, T. G.; Bibette, J.; Weitz, D. A. Elasticity of Compressed Emulsions. *Phys. Rev.*  
1010 *Lett.* **1995**, *75*, 2051.
- 1011 (70) Cloitre, M.; Borrega, R.; Leibler, L. Rheological Aging and Rejuvenation in Microgel  
1012 Pastes. *Phys. Rev. Lett.* **2000**, *85*, 4819.
- 1013 (71) O’Leary, L. E. R.; Fallas, J. A.; Bakota, E. L.; Kang, M. K.; Hartgerink, J. D. Multi-  
1014 Hierarchical Self-Assembly of a Collagen Mimetic Peptide from Triple Helix to  
1015 Nanofibre and Hydrogel. *Nat. Chem.* **2011**, *3*, 821–828.
- 1016 (72) Tirtaatmadja, V.; Ta, K. C.; Jenkins, R. D. Rheological Properties of Model Alkali-  
1017 Soluble Associative (HASE) Polymers: Effect of Varying Hydrophobe Chain Length.  
1018 *Macromolecules* **1997**, *30*, 3271–3282.
- 1019 (73) Raghavan, S. R.; Khan, S. A. Shear-induced Microstructural Changes in Flocculated  
1020 Suspensions of Fumed Silica. *J. Rheol. (N. Y. N. Y.)* **1995**, *39*, 1311.
- 1021 (74) Parthasarathy, M.; Klingenberg, D. J. Large Amplitude Oscillatory Shear of ER  
1022 Suspensions. *J. Nonnewton. Fluid Mech.* **1999**, *81*, 83–104.

- 1023 (75) Dudukovic, N. A.; Zukoski, C. F. Mechanical Properties of Self-Assembled Fmoc-  
1024 Diphenylalanine Molecular Gels. *Langmuir* **2014**, *30*, 4493–4500.
- 1025 (76) Menger, F. M.; Caran, K. L. Anatomy of a Gel. Amino Acid Derivatives That Rigidify  
1026 Water at Submillimolar Concentrations. *J. Am. Chem. Soc.* **2000**, *122*, 11679–11691.
- 1027 (77) Komatsu, H.; Ikeda, M.; Hamachi, I. Mechanical Reinforcement of Supramolecular  
1028 Hydrogel through Incorporation of Multiple Noncovalent Interactions. *Chem. Lett.*  
1029 **2011**, *40*, 198–200.
- 1030 (78) Clemente, M. J.; Fitremann, J.; Mauzac, M.; Serrano, J. L.; Oriol, L. Synthesis and  
1031 Characterization of Maltose-Based Amphiphiles as Supramolecular Hydrogelators.  
1032 *Langmuir* **2011**, *27*, 15236–15247.
- 1033 (79) Clemente, J.; Romero, P.; Serrano, J. L.; Fitremann, J.; Oriol, L. Supramolecular  
1034 Hydrogels Based on Glycoamphiphiles: Effect of the Disaccharide Polar Head. **2012**,  
1035 No. Lc.
- 1036 (80) Jung, J. H.; Rim, J. A.; Han, W. S.; Lee, S. J.; Lee, Y. J.; Cho, E. J.; Kim, J. S.; Ji, Q.;  
1037 Shimizu, T. Hydrogel Behavior of a Sugar-Based Gelator by Introduction of an  
1038 Unsaturated Moiety as a Hydrophobic Group. *Org. Biomol. Chem.* **2006**, *4*, 2033–  
1039 2038.
- 1040 (81) Adams, D. J.; Mullen, L. M.; Berta, M.; Chen, L.; Frith, W. J. Relationship between  
1041 Molecular Structure, Gelation Behaviour and Gel Properties of Fmoc-Dipeptides. *Soft*  
1042 *Matter* **2010**, *6*, 1971–1980.
- 1043 (82) Aufderhorst-Roberts, A.; Frith, W. J.; Donald, A. M. Micro-Scale Kinetics and  
1044 Heterogeneity of a PH Triggered Hydrogel. *Soft Matter* **2012**, *8*, 5940–5946.
- 1045 (83) Goddard, E. D. Ionizing Monolayers and PH Effects. *Adv. Coll. Interf. Sci.* **1974**, *4*,  
1046 45–78.
- 1047 (84) Ptak, M.; Egret-Charlier, M.; Sanson, A.; Bouloussa, O. A NMR Study of the  
1048 Ionization of Fatty Acids, Fatty Amines and N-Acylamino Acids Incorporated in  
1049 Phosphatidylcholine Vesicles. *Biochim. Biophys. Acta - Biomembr.* **1980**, *600*, 387–  
1050 397.
- 1051 (85) Cistola, D. P.; Hamilton, J. A.; Jackson, D.; Small, D. M. Ionization and Phase-  
1052 Behavior of Fatty-Acids in Water - Application of the Gibbs Phase Rule. *Biochemistry*  
1053 **1988**, *27*, 1881–1888.
- 1054 (86) Aufderhorst-Roberts, A.; Frith, W. J.; Kirkland, M.; Donald, A. M. Microrheology and  
1055 Microstructure of Fmoc-Derivative Hydrogels. *Langmuir* **2014**, *30*, 4483–4492.
- 1056 (87) Cuvier, A. S.; Babonneau, F.; Berton, J.; Stevens, C. V.; Fadda, G. C.; Genois, I.; Le

- 1057 Griel, P.; Péhau-Arnaudet, G.; Baccile, N. Synthesis of Uniform, Monodisperse,  
1058 Sophorolipid Twisted Ribbons. *Chem. - An Asian J.* **2015**, *10*, 2419–2426.
- 1059 (88) Raeburn, J.; Pont, G.; Chen, L.; Cesbron, Y.; Lévy, R.; Adams, D. J. Fmoc-  
1060 Diphenylalanine Hydrogels: Understanding the Variability in Reported Mechanical  
1061 Properties. *Soft Matter* **2012**, *8*, 1168–1174.
- 1062 (89) Baccile, N.; Selmane, M.; Le Griel, P.; Prévost, S.; Perez, J.; Stevens, C. V.; Delbeke,  
1063 E.; Zibek, S.; Guenther, M.; Soetaert, W.; et al. PH-Driven Self-Assembly of Acidic  
1064 Microbial Glycolipids. *Langmuir* **2016**, *32*, 6343–6359.
- 1065 (90) Bunton, C. A. *Reactions in Micelles and Similar Self-Organized Aggregates*, New  
1066 Compre.; Page, M. I., Ed.; Elsevier: Amsterdam - New York - Oxford, 1984; Vol. 6.
- 1067 (91) Manet, S.; Cuvier, A. S.; Valotteau, C.; Fadda, G. C.; Perez, J.; Karakas, E.; Abel, S.;  
1068 Baccile, N. Structure of Bolaamphiphile Sophorolipid Micelles Characterized with  
1069 SAXS, SANS, and MD Simulations. *J. Phys. Chem. B* **2015**, *119*, 13113–13133.
- 1070 (92) Huang, X.; Terech, P.; Raghavan, S. R.; Weiss, R. G. Kinetics of 5 $\alpha$ -Cholestan-3 $\beta$ -Yl  
1071 N-(2-Naphthyl)Carbamate/n-Alkane Organogel Formation and Its Influence on the  
1072 Fibrillar Networks. *J. Am. Chem. Soc.* **2005**, *127*, 4336–4344.
- 1073 (93) Toro-Vazquez, J. F.; Dibildox-Alvarado, E.; Charó-Alonso, M.; Herrera-Coronado, V.;  
1074 Gómez-Aldapa, C. a. The Avrami Index and the Fractal Dimension in Vegetable Oil  
1075 Crystallization. *J. Am. Oil Chem. Soc.* **2002**, *79*, 855–866.
- 1076 (94) Cuvier, A. S.; Babonneau, F.; Berton, J.; Stevens, C. V.; Fadda, G. C.; Genois, I.; Le  
1077 Griel, P.; Péhau-Arnaudet, G.; Baccile, N. Synthesis of Uniform, Monodisperse,  
1078 Sophorolipid Twisted Ribbons. *Chem. - An Asian J.* **2015**, *10*, 2419–2426.
- 1079  
1080  
1081  
1082  
1083  
1084  
1085

1086 **Table of Contents**

1087



1088